Eur. Phys. J. D **17**, 365–384 (2001)

THE EUROPEAN PHYSICAL JOURNAL D

EDP Sciences

Recoil-induced effects in a bidirectional ring laser

N. Piovella[1,a], V. Villa[1], R. Bonifacio[1], B.W.J. McNeil[2], and G.R.M. Robb[2]

[1] Dipartimento di Fisica, Università Degli Studi di Milano, INFN and INFM, Via Celoria 16, Milano 20133, Italy
[2] Department of Physics and Applied Physics, University of Strathclyde, Glasgow G4 0NG, Scotland, UK

Received 15 December 2000 and Received in final form 24 July 2001

Abstract. We present a theoretical study of a bidirectional ring laser in which the active medium is a cold atomic vapor. A novel feature of our analysis is the self-consistent description of the atomic motion due to recoil. It is shown that the evolution of the two counter-propagating fields within the cavity can be very different from that when recoil is neglected. We present an analytical study of the stationary unidirectional and bidirectional emission solutions and an analysis of their stability for a given average atomic velocity and Gaussian atomic velocity distribution. It is shown that the unidirectional emission solution is unstable if either the average velocity or the velocity distribution width is larger than a specific threshold value. If the mode frequency is resonant with the atoms, the symmetric bidirectional emission solution is stable. If the mode frequency is blue-detuned, the laser emits unidirectional pulses alternately in opposite directions. An initially inhomogeneously broadened medium in a blue-detuned ring laser experiences a continuous self-cooling process, which may reduce the atomic temperature down to the Doppler cooling limit. A simple analytical model interpreting the effect is presented.

PACS. 42.55.-f Lasers – 42.50.Vk Mechanical effects of light on atoms, molecules, electrons, and ions – 42.60.Mi Dynamical laser instabilities; noisy laser behavior

1 Introduction

In laser physics to date, the role of the translational motion of the particles comprising a gaseous active medium in the lasing process has been limited to Doppler broadening of the resonant transition. The effect of the laser radiation on the particles' translational motion through recoil is usually completely neglected for radiation wavelengths in the optical region of the spectrum and longer. In fact, at the usual temperatures of gaseous lasers, the Doppler broadening inhibits any regular motion of atoms due to atomic recoil. However, the continuous progress in optical cooling and trapping of atomic vapors has demonstrated the potentially important role of the mechanical effects of light on atomic dynamics.

In particular, there has been considerable interest in optical phenomena which can be directly related to atomic recoil *e.g.* the collective atomic recoil laser (CARL) [1,2] and recoil-induced resonances (RIR) [3,4]. In these phenomena, a probe field experiences gain while interacting with an ensemble of non-inverted two-level atoms that are simultaneously driven by an off-resonant pump field. In the CARL a collective instability leads to the formation of a strong matter grating (bunching), consisting of a large spatial modulation of the atomic density with a period equal to half of the radiation wavelength. Similar effects have been observed in theoretical studies of optical bistability [5,6] and superfluorescence [7] in cold atomic vapors.

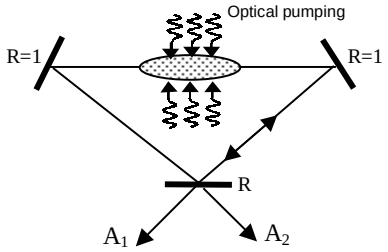

Fig. 1. A schematic diagram showing the atomic sample optically pumped and interacting with two counter-propagating modes A_1 and A_2 in a bidirectional ring cavity.

Recently, the study of recoil-induced optical phenomena has been extended [8,9] to a collection of *inverted* free atoms interacting with two radiation fields counter-propagating in a ring cavity, as schematically shown in Figure 1. The dynamics of the atoms and radiation fields are described using the semi-classical and one-dimensional CARL model [10] for an ensemble of free atoms in which a population inversion is induced by a transverse optical pump laser. A numerical study of these equations has shown [8] that if the excited atoms are initially cold and the effects of atomic recoil are treated self-consistently, the dynamical behavior of the ring laser can be significantly different from that when the effects of atomic recoil are neglected.

Bidirectional ring lasers have been studied for many years [11–13], in large part due to their application as laser

[a] e-mail: nicola.piovella@mi.infn.it

gyroscopes. It is well known [12] that, neglecting recoil, a homogeneously broadened ring laser admits two stationary solutions, a standing wave oscillation formed by two counter-propagating modes of equal intensity and a travelling wave oscillation consisting of a single-mode propagating in one direction. The coupling between the two modes is provided by the scattering from the spatial grating formed in the population difference. The bidirectional solution is unstable and the unidirectional solution is stable if the cavity decay rates are equal and much smaller than the atomic relaxation rates (good cavity limit). However, if the atoms are left free to recoil due to the radiation emission [8], then the Doppler shift due to the average atomic velocity affects the stability of the stationary solutions. On resonance, the unidirectional solution becomes unstable and the bidirectional solution stable, whereas by detuning the frequency of the cavity mode above the atomic resonance ("blue-detuning"), a pulsed regime may occur, with unidirectional emission alternately in opposite directions. When the frequency of the cavity mode is detuned below the resonance ("red-detuning"), the effect of recoil is to drive the laser below threshold.

This paper investigates in detail the effects of atomic motion on the ring laser emission. The analysis includes an analytical study of the stationary solutions and their stability for a medium with homogeneous broadening (*i.e.* cold atoms) and inhomogeneous broadening (*i.e.* with a finite width of the initial velocity distribution). In particular, we demonstrate that on resonance, the bidirectional solution is stable when the Doppler shift due to the recoil velocity parallel to the field propagation axis, $k\langle v_z\rangle$ (where $k = \omega/c$ is the radiation wavenumber), becomes comparable to the natural atomic linewidth, $\gamma_\perp$, such that the two modes can be considered uncoupled. A similar mechanism is responsible for the pulsed emission in the blue-detuned case. The analysis shows that in general the ring laser allows for stationary unidirectional as well as bidirectional emission, with equal mode intensities (symmetric emission) or different mode intensities (asymmetric emission). However, the stability of the stationary solutions is strongly affected by the coherent motion induced by recoil as well as by the incoherent motion due to thermal velocity spread. We give a detailed picture of the dependence of the laser stability on the main parameters such as gain, detuning, mean velocity and velocity spread. When the effect of the laser emission on the atomic motion is considered in a medium with initial finite width of the velocity distribution, we observe a novel self-cooling effect within the inverted atomic system, with a narrowing of the velocity distribution curve. When the laser is tuned to resonance, self-cooling occurs only during the transient between the unidirectional emission (unstable) and the bidirectional emission (stable), leading to only a slight decrease of the atomic velocity spread. The self-cooling process is much more efficient when the laser is blue-detuned. Although in this case the atoms lase periodically in opposite directions, the cooling process is independent of which mode is emitted, and a monotonic decrease of the velocity spread is observed. During the cooling process, the average atomic velocity oscillates around zero, making the cooling trap translationally stable. For these reasons, the method appears particularly promising for cooling a warm gas, pumped with some "velocity-preserving" method (for instance using a pump laser exciting the atomic sample in a transverse direction with respect to the cavity propagation axes) to a very low temperature (near the Doppler limit determined by momentum diffusion).

The paper is organized as follows: Section 2 describes the background to the classical bidirectional ring laser problem. Section 3 outlines the complete self-consistent model for a system with population inversion and interacting with two counter-propagating modes of a bidirectional ring cavity. In Section 4 the general model is reduced, using a Fourier expansion in space of the internal atomic variables, to two equations for the mode intensities, describing the laser dynamics for an assigned, constant state of atomic motion. The stationary solutions of these equations are discussed in Section 5 and their stability is analyzed in Section 6. In Section 7 numerical calculations of the self-consistent dynamics with recoil are presented and compared with the analytical results, together with a simple analytical model interpreting the self-cooling process. Finally, in Section 8 we shortly discuss the possibility of an experimental observation of the predicted effects.

2 Background

Laser theory has attracted a large number of studies centered on the stability problem [14]. The motivations for these studies were both theoretical, the laser equations being simple enough that they can be derived from first principles with a minimum of phenomenology, and practical, the laser stability being essential when the laser is used as a tool in scientific or industrial applications. The bidirectional operation of ring lasers is of particular interest because of their use as gyroscopes [15] wherein the frequencies of the two counter-propagating modes are split by any rotation of the plane of the laser about an axis normal to the plane. However, it is well known that in a homogeneously broadened ring laser mode competition induced by population grating formation suppresses one of the modes [12]. A large class of studies [16] focussed on the so-called "second-instability" of lasers in the "bad-cavity limit", *i.e.* when the cavity decay rate κ_c exceeds the atomic spontaneous decay $\gamma_\perp$, so that the usual adiabatic elimination of the atomic variables is not valid. A rich class of dynamical behaviors were found when the lasers are detuned from resonance [17] or when unequal losses for the two modes are produced inside the resonator [13]. In all these studies the average motion of the center-of-mass of the atoms due to recoil has been neglected, being masked by the inhomogeneous broadening of the resonance due, for a gas system, to the thermal Doppler motion.

The recent improved cooling methods of atomic systems has renewed interest in atom-field interactions at low temperature, where the effects of atomic recoil cannot be neglected. Indeed, dense samples of atoms in a Bose-Einstein Condensate (BEC) are systems where the

thermal broadening is almost completely absent [18]. For these systems, the atomic motion is in general not classical, and a quantum model of CARL [19] should be used. However, a classical description of the atomic motion in BECs may still be used when the average number of photons scattered per atom is large [20]. Although until now all experiments have been performed exposing the atomic sample to off-resonant laser sources [21], in order not to heat the system, it is reasonable to imagine that in the near future it will be possible to perform laser experiments with cold atoms in which a population inversion has been produced.

3 Model

The model used to describe the interaction is one-dimensional and semi-classical. The internal atomic dynamics (dipole moment and population difference) are described in terms of a quantum-mechanical two-level system and the external atomic dynamics (position and momentum) are treated classically, with the atoms as point particles. The equations used to describe the atom-field interaction within the cavity extend the usual Maxwell-Bloch model [22] to self-consistently include the atomic center-of-mass motion. This extended model was introduced originally to describe CARL [1] and the spontaneous formation of a longitudinal density grating in a cold atomic system irradiated by a detuned pump laser [23]. For these reasons we refer to it as "the CARL model". It assumes that the radiation electric field is the sum of two counter-propagating, linearly polarized radiation modes of equal frequency $\omega = ck$, $E(z,t) = \mathcal{E}_1(z,t)\mathrm{e}^{\mathrm{i}(kz-\omega t)} + \mathcal{E}_2(z,t)\mathrm{e}^{-\mathrm{i}(kz+\omega t)} + \text{c.c.}$, where z is the propagation axis and subscripts $1,2$ refer to the clockwise and anti-clockwise propagating fields, respectively. The two fields are close to resonance with the transition frequency $\omega_0 = (E_b - E_a)/\hbar$ between the lower state $|a\rangle$ and the upper state $|b\rangle$. The density matrix elements $\rho_{mn}, (m,n = a,b)$ describe the internal evolution of each atom, considered as a two-level system. The off-diagonal elements ($\rho_{ba} = \rho_{ab}^*$) describe the polarization as induced by the counter-propagating fields. The dipole moment along the polarization axis of the electric field is $d = \mu(\rho_{ab} + \rho_{ba})$, where μ is the dipole matrix element. The off-diagonal elements ρ_{ab} may be written conveniently as a sum of two polarization waves, $\rho_{ab} = S_1(z,t)\mathrm{e}^{\mathrm{i}(kz-\omega t)} + S_2(z,t)\mathrm{e}^{-\mathrm{i}(kz+\omega t)}$.

Special attention should be given to the assumption that a population inversion is obtained in the atoms. We assume that the atomic system is *closed*, in the sense that the sum of the populations of the energy levels involved in the pumping cycle is conserved for each velocity subclass of atoms. We assume that the atoms consist of three-level systems where only the transition between the two excited levels $|a\rangle$ and $|b\rangle$ are driven by the two radiation modes propagating within the cavity. Population inversion is obtained by exposing the sample to a laser incident in a transverse direction with respect to the z-axes (see Fig. 1) and resonant with the transition between the ground state

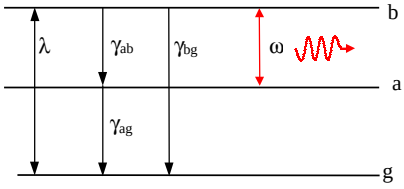

Fig. 2. A schematic energy level diagram of the atoms.

$|g\rangle$ and the upper state $|b\rangle$, with a pump rate λ (see Fig. 2). We define $D = \rho_{bb} - \rho_{aa}$ as the population difference between the upper $|b\rangle$ and lower $|a\rangle$ states involved in the interaction, D^{eq} as the equilibrium value in the presence of the pump laser alone and $\gamma_\parallel$ the relaxation rate of the population difference. The explicit expression of D^{eq} and $\gamma_\parallel$ are given in Appendix A.

Use of the definitions above in the Bloch equations describing the two-level atomic system, the equation for the force on the atom at $z = z(t)$, $F(t) = d\,[\partial_z E(z,t)]_{z=z(t)}$, and the Maxwell wave equations, yield the CARL equations [10]:

$$\frac{\mathrm{d}S_1(\theta,t)}{\mathrm{d}t} = -\gamma_\perp[1-\mathrm{i}(\delta-\beta)]S_1(\theta,t) - \mathrm{i}\frac{\mu}{\hbar}D(\theta,t)\mathcal{E}_1(t) \quad (1)$$

$$\frac{\mathrm{d}S_2(\theta,t)}{\mathrm{d}t} = -\gamma_\perp[1-\mathrm{i}(\delta+\beta)]S_2(\theta,t) - \mathrm{i}\frac{\mu}{\hbar}D(\theta,t)\mathcal{E}_2(t) \quad (2)$$

$$\begin{aligned}\frac{\mathrm{d}D(\theta,t)}{\mathrm{d}t} &= -\gamma_\parallel[D(\theta,t) - D^{\mathrm{eq}}] \\ &\quad -2\mathrm{i}\frac{\mu}{\hbar}\Big\{\mathcal{E}_1(t)^*\left[S_1(\theta,t) + S_2(\theta,t)\mathrm{e}^{-\mathrm{i}\theta}\right] \\ &\quad +\mathcal{E}_2(t)^*\left[S_2(\theta,t) + S_1(\theta,t)\mathrm{e}^{\mathrm{i}\theta}\right] - \text{c.c.}\Big\} \quad (3)\end{aligned}$$

$$\frac{\mathrm{d}\theta}{\mathrm{d}t} = 2\gamma_\perp\beta \quad (4)$$

$$\begin{aligned}\frac{\mathrm{d}\beta}{\mathrm{d}t} &= -\mathrm{i}\frac{\omega_{\mathrm{r}}\mu}{2\gamma_\perp\hbar}\Big\{\mathcal{E}_1(t)^*\left[S_1(\theta,t) + S_2(\theta,t)\mathrm{e}^{-\mathrm{i}\theta}\right] \\ &\quad -\mathcal{E}_2(t)^*\left[S_2(\theta,t) + S_1(\theta,t)\mathrm{e}^{\mathrm{i}\theta}\right] - \text{c.c.}\Big\} \quad (5)\end{aligned}$$

$$\frac{\mathrm{d}\mathcal{E}_1(t)}{\mathrm{d}t} = \mathrm{i}\frac{\omega n\mu}{2\epsilon_0}\left\langle S_1(\theta,t) + S_2(\theta,t)\mathrm{e}^{-\mathrm{i}\theta}\right\rangle - \kappa_{\mathrm{c}}\mathcal{E}_1 \quad (6)$$

$$\frac{\mathrm{d}\mathcal{E}_2(t)}{\mathrm{d}t} = \mathrm{i}\frac{\omega n\mu}{2\epsilon_0}\left\langle S_2(\theta,t) + S_1(\theta,t)\mathrm{e}^{\mathrm{i}\theta}\right\rangle - \kappa_{\mathrm{c}}\mathcal{E}_2. \quad (7)$$

In these equations $\theta = 2kz$ is the scaled atomic coordinate, $\beta = kv_z/\gamma_\perp$ is the scaled atomic velocity, $\delta = (\omega - \omega_0)/\gamma_\perp$ is the scaled field-atom detuning, $\omega_{\mathrm{r}} = 2\hbar k^2/M$ is the recoil frequency, $\gamma_\perp$ and $\gamma_\parallel$ are the decay rates of polarization and population difference, respectively, M is the atomic mass, $n = n_{\mathrm{s}}(L_{\mathrm{s}}/L_{\mathrm{cav}})$ is the 'reduced' atomic density in the cavity, n_{s} is the atomic density of the sample, L_{s} is the sample length and L_{cav} is the cavity length. In deriving equations (1–7) we have assumed that the mean field limit can be applied when describing the evolution of the two modes circulating in the cavity. Cavity losses are assumed to be equal for both modes and $\kappa_{\mathrm{c}} = -(c/L_{\mathrm{cav}})\ln(R) = \omega/2Q$ is the loss rate for a cavity with reflection coefficient R and quality factor Q. It has been assumed that the radiation frequency coincides with that of a mode of the cavity *i.e.* $\omega = \omega^{(m)} = 2\pi mc/L_{\mathrm{cav}}$ where m is an integer. The atoms are labeled by their

initial position and velocity, θ_0 and β_0, and the mean in the equations (6, 7) is defined as

$$\langle X(\theta,\beta)\rangle = \frac{1}{2\pi}\int_0^{2\pi} \mathrm{d}\theta_0 \times \int_{-\infty}^{\infty} \mathrm{d}\beta_0 f(\beta_0) X(\theta(\theta_0,p_0,t),\beta(\theta_0,\beta_0,t)). \quad (8)$$

We assume that the initial phases θ_0 are uniformly distributed over 2π and that the velocities are Doppler-broadened with a Gaussian distribution $f(\beta_0) = (1/\sigma\sqrt{2\pi})\exp[-\beta_0^2/2\sigma^2]$, where $\sigma = k\sigma_\mathrm{v}/\gamma_\perp$ and $\sigma_\mathrm{v} = \sqrt{k_\mathrm{B}T/M}$ is the standard deviation of the velocity along the cavity axis, k_B is the Boltzmann's constant and T the gas temperature.

From equations (1–7) it is possible to obtain the equations for the rate of exchange of average momentum, energy and momentum spread:

$$\frac{\mathrm{d}}{\mathrm{d}t}\left(2\frac{\gamma_\perp}{\omega_\mathrm{r}}\langle\beta\rangle + N_1 - N_2\right) = -2\kappa_\mathrm{c}(N_1 - N_2) \quad (9)$$

$$\frac{\mathrm{d}}{\mathrm{d}t}\left(\frac{\langle D\rangle}{2} + N_1 + N_2\right) = -\frac{\gamma_\parallel}{2}(\langle D\rangle - D^\mathrm{eq}) - 2\kappa_\mathrm{c}(N_1+N_2) \quad (10)$$

$$\frac{\mathrm{d}}{\mathrm{d}t}\left[\frac{\gamma_\perp}{\omega_\mathrm{r}}\langle\beta^2\rangle + (\delta - 2\epsilon\Omega_1)N_1 + (\delta - 2\epsilon\Omega_2)N_2\right] = -2\Big\{[\delta - (1+\epsilon)\Omega_1]N_1 + [\delta - (1+\epsilon)\Omega_2]N_2\Big\} \quad (11)$$

where $N_{1,2} = 2\epsilon_0|\mathcal{E}_{1,2}|^2/\hbar\omega n$ is the average number of emitted photons per atom in modes 1 and 2, respectively, $\epsilon = \kappa_\mathrm{c}/\gamma_\perp$, $\Omega_{1,2} = \kappa_\mathrm{c}^{-1}\dot{\phi}_{1,2}$, and $\dot{\phi}_{1,2}$ is the time derivative of the phase of the complex amplitudes $\mathcal{E}_{1,2} = |\mathcal{E}_{1,2}|\mathrm{e}^{\mathrm{i}\phi_{1,2}}$. Equations (9, 10) follow from the conservation of momentum and number of excitations. Equation (11) connects the velocity spread $\sigma = (\langle\beta^2\rangle - \langle\beta\rangle^2)^{1/2}$ to the frequency shift $\Omega_{1,2}$ and will be important in the discussion of the self-cooling mechanism (see Sect. 7.2).

4 Analysis

Preliminary results showing the effects of recoil in a ring laser were obtained solving equations (1–7) numerically for a cold atomic vapor [8]. In particular, the numerical simulations showed that the spontaneous formation of a density grating (*i.e.* bunching) along the cavity axis (fundamental in CARL-like effects and responsible for the pump-probe gain mechanism in CARL), does not play an important role in a ring laser. In fact, a density grating forms only in the transient regime and it becomes negligible after saturation. This occurs for two main reasons: initially the emission is bidirectional, and the pendulum potential resulting from interference of the two counter-propagating fields of equal intensity bunches the atoms. However, the bidirectional emission becomes unstable near saturation, and one of the two fields is suppressed by mode competition [12]. As a consequence, the atoms are no longer trapped by the potential and the bunching rapidly disappears. The second mechanism which destroys the bunching also during bidirectional emission is due to the modulation of the population difference D which deforms the pendulum potential, flattening its minimum and allowing the atoms to spread out in position.

The aim of this paper is twofold: (1) to give an analytical description of the effect of the atomic motion in a ring laser; (2) to extend the analysis to an inhomogeneously broadened (*i.e.* Doppler broadened) medium. The first goal is obtained introducing approximations and assumptions that reduce the basic equations to a low-dimensional model for only the two radiation mode intensities, the average atomic velocity and the velocity spread. This allows us to study the stationary solutions and the stability of the two radiation modes analytically for a given (*i.e.* fixed) atomic motional state. Then, the results are compared with the numerical solution of the basic equations. Three main approximations are assumed: (a) no density modulation occurs during the long-term evolution of the ring laser, *i.e.* the atomic phases θ are assumed always uniformly distributed over 2π; (b) the cavity loss κ_c is much less than the atomic linewidths $\gamma_\perp$ and $\gamma_\parallel$ ("good-cavity limit"); (c) the velocity distribution remains always Gaussian, *i.e.* the interaction with the electromagnetic fields changes only the average velocity $\langle\beta\rangle$ and the distribution width σ and not the Gaussian shape of the velocity distribution. We note that assumption (a) is fundamental in order to obtain an analytical description of the effects of the average and thermal motions on the laser emission, and is justified by numerical evidence. The second assumption (b) allows for the adiabatic elimination of the two atomic polarizations and population inversion. Finally, the last assumption (c), perhaps the most difficult to be accepted on the basis of theoretical or intuitive arguments, will be tested numerically comparing the results of the reduced model with those obtained from the exact equations. We note that assumption (c) does not influence the analytical results, which are obtained for a given (*i.e.* uniform) motional state. Then, the dynamics with recoil are investigated by integrating the exact equations numerically. However, if assumption (c) is valid, it can allow for a useful reduction of the exact equations to a low-dimensional model.

We begin our analysis introducing $S_{1,2} = s_{1,2}\exp(\mathrm{i}\phi_{1,2})$, so that equations (1–3, 6, 7) become:

$$\dot{s}_1(\theta,t) = -\gamma_\perp(1-\mathrm{i}\delta_1)s_1(\theta,t) - \mathrm{i}\frac{\mu|\mathcal{E}_1|}{\hbar}D(\theta,t) \quad (12)$$

$$\dot{s}_2(\theta,t) = -\gamma_\perp(1-\mathrm{i}\delta_2)s_2(\theta,t) - \mathrm{i}\frac{\mu|\mathcal{E}_2|}{\hbar}D(\theta,t) \quad (13)$$

$$\dot{D}(\theta,t) = -\gamma_\parallel(D(\theta,t) - D^\mathrm{eq}) - 2\mathrm{i}\frac{\mu}{\hbar}\left[|\mathcal{E}_1|\left(s_1 + s_2\,\mathrm{e}^{-\mathrm{i}\psi}\right) + |\mathcal{E}_2|\left(s_2 + s_1\,\mathrm{e}^{\mathrm{i}\psi}\right) - \mathrm{c.c.}\right] \quad (14)$$

$$|\dot{\mathcal{E}}_1| = -\frac{\omega n\mu}{2\epsilon_0}\mathrm{Im}\left\langle s_1 + s_2\,\mathrm{e}^{-\mathrm{i}\psi}\right\rangle - \kappa_\mathrm{c}|\mathcal{E}_1| \quad (15)$$

$$\Omega_1|\mathcal{E}_1| = \frac{\omega n\mu}{2\kappa_\mathrm{c}\epsilon_0}\mathrm{Re}\left\langle s_1 + s_2\,\mathrm{e}^{-\mathrm{i}\psi}\right\rangle \quad (16)$$

$$\frac{\mathrm{d}x_{1,2}}{\mathrm{d}\tau}+x_{1,2}=\int \mathrm{d}\beta\left\{\frac{f(\beta)g_{1,2}\left[x_{1,2}+\sqrt{x_1x_2}\,(\mathrm{Re}(z_0)\mp\delta_{1,2}\mathrm{Im}(z_0))\right]}{1+g_1x_1+g_2x_2+\sqrt{x_1x_2}\left[(g_1+g_2)\mathrm{Re}(z_0)+(\delta_2g_2-\delta_1g_1)\mathrm{Im}(z_0)\right]}\right\}, \tag{36}$$

$$\Omega_{1,2}x_{1,2}=\int \mathrm{d}\beta\left\{\frac{f(\beta)g_{1,2}\left[\delta_{1,2}x_{1,2}+\sqrt{x_1x_2}\,(\delta_{1,2}\mathrm{Re}(z_0)\pm\mathrm{Im}(z_0))\right]}{1+g_1x_1+g_2x_2+\sqrt{x_1x_2}\left[(g_1+g_2)\mathrm{Re}(z_0)+(\delta_2g_2-\delta_1g_1)\mathrm{Im}(z_0)\right]}\right\}, \tag{37}$$

$$|\dot{\mathcal{E}}_2|=-\frac{\omega n\mu}{2\epsilon_0}\mathrm{Im}\left\langle s_2+s_1\,\mathrm{e}^{\mathrm{i}\psi}\right\rangle-\kappa_\mathrm{c}|\mathcal{E}_2| \tag{17}$$

$$\Omega_2|\mathcal{E}_2|=\frac{\omega n\mu}{2\kappa_\mathrm{c}\epsilon_0}\mathrm{Re}\left\langle s_2+s_1\,\mathrm{e}^{\mathrm{i}\psi}\right\rangle \tag{18}$$

where a dot indicates the derivative with respect to t, $\psi=\theta+\phi_1-\phi_2$ and $\delta_{1,2}=\delta\mp\beta-\epsilon\Omega_{1,2}$ are the effective atom-field detunings. We observe that the atomic motion introduces rapid temporal variations in the functions s_1, s_2 and D, making the solution much more complicated than the case when the atomic motion is neglected. Although these temporal variations are averaged in the field equations (15–18), their presence considerably modifies the solution. To treat the problem with a rapid varying phase ψ, we expand s_1, s_2 and D in Fourier series [11]:

$$s_1=\sum_{-\infty}^{+\infty}p_n\mathrm{e}^{\mathrm{i}n\psi} \tag{19}$$

$$s_2=\sum_{-\infty}^{+\infty}q_n\mathrm{e}^{\mathrm{i}n\psi} \tag{20}$$

$$D=\sum_{-\infty}^{+\infty}d_n\mathrm{e}^{\mathrm{i}n\psi}, \tag{21}$$

where $d_n^*=d_{-n}$ because D is real. Inserting these in equations (12–14), and assuming $\dot{p}_n\ll\gamma_\perp p_n$, $\dot{q}_n\ll\gamma_\perp q_n$ and $\dot{d}_n\ll\gamma_\parallel d_n$, yields

$$p_n=-\mathrm{i}\frac{\mu|\mathcal{E}_1|}{\hbar\gamma_\perp}\frac{d_n}{1-\mathrm{i}[\delta_1-n\Omega]} \tag{22}$$

$$q_n=-\mathrm{i}\frac{\mu|\mathcal{E}_2|}{\hbar\gamma_\perp}\frac{d_n}{1-\mathrm{i}[\delta_1+(1-n)\Omega]} \tag{23}$$

and

$$\begin{aligned}(1+\mathrm{i}n\gamma\Omega)d_n=D^\mathrm{eq}\delta_{n,0}&\\-2\mathrm{i}\frac{\mu}{\hbar\gamma_\parallel}&\left[|\mathcal{E}_1|(p_n-p_{-n}^*+q_{n+1}-q_{1-n}^*)\right.\\&\left.+|\mathcal{E}_2|(q_n-q_{-n}^*+p_{n-1}-p_{-1-n}^*)\right],\end{aligned} \tag{24}$$

where $\Omega=\dot{\psi}=2\beta+\epsilon(\Omega_1-\Omega_2)$, $\gamma=\gamma_\perp/\gamma_\parallel$ and we used the relation $\delta_2=\delta_1+\Omega$. Let us now introduce the complex coefficients:

$$\alpha_n=1+\mathrm{i}n\gamma\Omega+g_1[x_1\mathcal{L}_{n,-n}+x_2\mathcal{L}_{1+n,1-n}] \tag{25}$$

$$\beta_n=g_1\sqrt{x_1x_2}\mathcal{L}_{n,1-n}, \tag{26}$$

where

$$x_{1,2}=\frac{8\epsilon_0\kappa_\mathrm{c}|\mathcal{E}_{1,2}|^2}{\hbar\omega nD^\mathrm{eq}\gamma_\parallel}=\frac{4\kappa_\mathrm{c}N_{1,2}}{\gamma_\parallel D^\mathrm{eq}} \tag{27}$$

are the dimensionless intensities of the mode 1 and 2, respectively,

$$g_{1,2}=\frac{g_0}{1+\delta_{1,2}^2} \tag{28}$$

are the gain to loss ratios relative to the two modes, $g_0=\omega n\mu^2D^\mathrm{eq}/2\epsilon_0\hbar\gamma_\perp\kappa_\mathrm{c}$ and

$$\mathcal{L}_{n,m}=\frac{1+\delta_1^2}{2}\left[\frac{1}{1+\mathrm{i}(\delta_1+n\Omega)}+\frac{1}{1-\mathrm{i}(\delta_1+m\Omega)}\right]. \tag{29}$$

With these definitions and equations (22) and (23), equation (24) can be written as:

$$\alpha_nd_n=D^\mathrm{eq}\delta_{n,0}-(\beta_nd_{n-1}+\beta_{n+1}d_{n+1})\,. \tag{30}$$

In particular, for $n=0$, $\alpha_0d_0=D^\mathrm{eq}-2\mathrm{Re}(\beta_1d_1)$. Dividing by d_n, for $n\neq0$, and introducing the new unknown $z_n=d_{n+1}/d_n$, equation (30) yields

$$z_{n-1}=\frac{-\beta_n}{\alpha_n+\beta_{n+1}z_n}\,. \tag{31}$$

Setting $n=1$ and iterating equation (31), we obtain an expression for z_0 in the form of an infinite continued fraction [24]:

$$z_0=\frac{-\beta_1}{\alpha_1+}\,\frac{-\beta_2}{\alpha_2+}\cdots \tag{32}$$

Once z_0 is calculated numerically using an iterative method, it is possible to evaluate all the other Fourier components d_n of the population difference:

$$d_0=\frac{D^\mathrm{eq}}{\alpha_0+2\mathrm{Re}(\beta_1z_0)} \tag{33}$$

$$d_1=d_0z_0 \tag{34}$$

$$d_{n+1}=-\frac{\beta_nd_{n-1}+\alpha_nd_n}{\beta_{n+1}}. \tag{35}$$

Finally, using the relations

$$\frac{1}{2\pi}\int_0^{2\pi}\mathrm{d}\psi(s_1+s_2\,\mathrm{e}^{-\mathrm{i}\psi})=p_0+q_1$$

$$\frac{1}{2\pi}\int_0^{2\pi}\mathrm{d}\psi(s_2+s_1\,\mathrm{e}^{\mathrm{i}\psi})=q_0+p_{-1}$$

and (22, 23), equations (15–18) give:

see equations (36, 37) above,

where we have introduced the dimensionless cavity time $\tau=2\kappa_\mathrm{c}t$. The usual approximation in which the population difference and the two polarization waves are adiabatically eliminated has been generalized to their Fourier

amplitudes, in order to describe the effects of the atomic motion. The assumption that the Fourier amplitudes p_n, q_n and d_n are slowly varying is justified by the fact that the rate of change of the fields is of the order of κ_c and we assume $\kappa_c \ll \gamma_\perp, \gamma_\parallel$. The original equations have been reduced to a set of two differential equations for the mode intensities x_1 and x_2 and two algebraic equations for the phase shifts Ω_1 and Ω_2, together with the equations for the atomic center-of-mass motion (4, 5). The problem may be further approximated assuming that the velocity distribution, $f(\beta)$, does not change its shape appreciably when the atoms vary their velocity β due to recoil. Because the active medium is an atomic gas, Doppler broadening imposes that $f(\beta)$ is a Gaussian function with center $\langle\beta\rangle$ and variance $\sigma^2 = \langle\beta^2\rangle - \langle\beta\rangle^2$, whose evolution is given by equations (9) and (11). We limit the analysis to the "good cavity" regime, $\kappa_c \ll \gamma_\perp$, in which the frequency shifts $\Omega_{1,2}$ have a negligible effect on the laser emission. In fact, from equations (36) and (37), it follows that $\Omega_{1,2}$ is of the order of $\delta_{1,2}$, so that, for $\epsilon \ll 1$, $\delta_{1,2} \approx \delta \mp \beta$ and $\Omega \approx 2\beta$. Equations (9) and (11) can be written, for $\epsilon \ll 1$ and introducing the dimensionless intensities (27), in the form:

$$(\mathrm{d}/\mathrm{d}\tau)[\tau_r\beta_0 + x_1 - x_2] = -x_1 + x_2 \tag{38}$$

$$(\mathrm{d}/\mathrm{d}\tau)[(\tau_r/2)(\sigma^2 + \beta_0^2) + \delta(x_1 + x_2)] = - [(\delta - \Omega_1)x_1 + (\delta - \Omega_2)x_2], \tag{39}$$

where $\beta_0 = \langle\beta\rangle$ and $\tau_r = (4\gamma/D^{eq})(2\kappa_c/\omega_r)$ is the recoil time in units of the cavity time, $(2\kappa_c)^{-1}$. The assumption that the atomic velocities remain normally distributed also when the atoms experience recoil is reasonably true when the atomic positions are uniformly distributed, *i.e.* no bunching is present. Otherwise space-velocity correlations will strongly modify the velocity distribution $f(\beta)$. Neglecting other mechanisms (*e.g.* momentum diffusion) that could appreciably change the velocity distribution, it is reasonable to assume that atomic recoil influences only the first two moments of the distribution, *i.e.* β_0 and σ. Hence, an approximated description of the dynamical evolution of the two laser modes and of the atomic motion in a ring laser can be obtained by solving the reduced system of equations (36–39). We will check this point numerically in Section 7.

In the following, we discuss the stationary solutions of equation (36) and their stability in the presence of an uniform atomic motion, for a homogeneously and inhomogeneously broadened medium. In the former case, we assume cold atoms, with $f(\beta) = \delta(\beta - \beta_0)$. In the second case, we assume a gas sample with Doppler broadening, described by

$$f(\beta) = \frac{1}{\sigma\sqrt{2\pi}} \mathrm{e}^{-(\beta-\beta_0)^2/2\sigma^2}. \tag{40}$$

The solutions will be studied as a function of the following four parameters characterizing the ring laser operation: g_0, δ, β_0 and σ. The aim of this study is to investigate the effect of a given atomic motion (*i.e.* with constant velocity) on the ring laser operation. The results of this analysis will be useful to understand in Section 7 the self-consistent dynamics with recoil, where the atomic motion evolves under the influence of the radiation fields.

5 Stationary solutions

Equation (36) admit in general two distinct classes of non-trivial stationary solutions: the unidirectional solution, with either $x_1 = 0$ or $x_2 = 0$, and the bidirectional solution, with both x_1 and x_2 different from zero. Furthermore, the bidirectional solution may be symmetric, with $x_1 = x_2$, or asymmetric, with $x_1 \neq x_2$. We discuss each stationary solution separately. Before proceeding, we note that x_2 is a solution of the same equation as that for x_1 with the sign of δ changed. In fact, if $\delta \to -\delta$, then $\delta_1 \to -\delta_2$ and the equation (36) for the modes 1 and 2 coincide. Hence, it will be sufficient to solve the equation for x_1 alone and obtain x_2 from x_1 just changing the sign of δ.

5.1 Unidirectional solution

Assuming $x_2 = 0$ in equation (36), the stationary solution x_1 is the solution of the following implicit equation,

$$1 = g_0 \int \mathrm{d}\beta \frac{f(\beta)}{1 + g_0 x_1 + (\delta - \beta)^2}\,. \tag{41}$$

Using equation (41) in equation (37), we obtain

$$\Omega_1 = \delta - g_0 \int \mathrm{d}\beta \frac{\beta f(\beta)}{1 + g_0 x_1 + (\delta - \beta)^2}\,. \tag{42}$$

From (41) and (42) we observe that in the limit of large gain, $g_0 \gg 1$, $x_1 \approx 1$ and $\Omega_1 \approx \delta - \beta_0$. For homogeneous broadening, *i.e.* $f(\beta) = \delta(\beta - \beta_0)$,

$$x_1 = 1 - \frac{1 + (\delta - \beta_0)^2}{g_0} \tag{43}$$

and $\Omega_1 = \delta - \beta_0$, whereas for Doppler broadening, with $f(\beta)$ given by equation (40), x_1 is the solution of the implicit equation [25]

$$\xi\sigma = g_0\sqrt{\frac{\pi}{2}}\mathrm{Re}\ W\left(\frac{\delta - \beta_0 + \mathrm{i}\xi}{\sqrt{2}\sigma}\right) \tag{44}$$

and, from (42),

$$\Omega_1 = \delta - \beta_0 - \frac{g_0}{\sigma}\sqrt{\frac{\pi}{2}}\mathrm{Im}\ W\left(\frac{\delta - \beta_0 + \mathrm{i}\xi}{\sqrt{2}\sigma}\right), \tag{45}$$

where W is defined by $W(z) = \exp(-z^2)\mathrm{erfc}(-\mathrm{i}z)$ and $\xi = \sqrt{1 + g_0 x_1}$.

5.2 Symmetric bidirectional solution

A detailed discussion about the properties of the bidirectional solution is contained in Appendix B. The main result is that when $\delta = 0$ and the laser is above threshold, the symmetric bidirectional solution (with $x_1 = x_2 = x$) is always a stationary solution of equation (36). It is a stationary solution also for $\delta \neq 0$, but only for the case of homogeneous broadening and stationary atoms ($\beta_0 = 0$). In this last case, equation (31) is independent of the index n and z_0 can be evaluated explicitly. A straightforward calculation gives

$$x = \frac{1}{2}\left[1 - \frac{1}{4g_1}\left(1 + \sqrt{1+8g_1}\right)\right],$$

where now $g_1 = g_0/(1+\delta^2)$. For the case of inhomogeneous broadening and $\delta = 0$, x is the solution of the implicit equation

$$1 = g_0 \int \mathrm{d}\beta f(\beta) \frac{1 + Z(\beta)}{1 + \beta^2 + 2g_0 x[1 + Z(\beta)]}, \qquad (46)$$

where $Z(\beta) = \mathrm{Re}z_0 + \beta \mathrm{Im}z_0$. We observe that for large gain ($g_0 \gg 1$), $x \approx 1/2$. For homogeneous broadening, equation (46) can be written as

$$x = \frac{1}{2}\left\{1 - \frac{1 + \beta_0^2}{g_0[1 + Z(\beta_0)]}\right\}. \qquad (47)$$

5.3 Asymmetric bidirectional solution

The asymmetric bidirectional solution, with both x_1 and x_2 different from zero and $x_1 \neq x_2$, can be a stationary solution for homogeneous broadening if both δ and β_0 are different from zero, and for inhomogeneous broadening if δ is different from zero. It can also be a solution for an inhomogeneously broadened laser with $\delta = 0$, if x_1 and x_2 satisfy the following system of equations:

$$1 = g_0 \int \mathrm{d}\beta \frac{f(\beta)}{1 + \beta^2 + g_0[x_1 + x_2 + 2\sqrt{x_1 x_2} Z(\beta)]} \qquad (48)$$

$$0 = \int \mathrm{d}\beta \frac{f(\beta) Z(\beta)}{1 + \beta^2 + g_0[x_1 + x_2 + 2\sqrt{x_1 x_2} Z(\beta)]}. \qquad (49)$$

Figure 3 shows the asymmetric bidirectional solution for homogeneous broadending and $g_0 = 50$, obtained by iteration of the stationary equation (36) with $\mathrm{d}x_{1,2}/\mathrm{d}\tau = 0$: the mode amplitudes x_1 (continuous line) and x_2 (dashed line) are plotted against δ for $\beta_0 = -3$ (Fig. 3a) and against β_0 for $\delta = -1$ (Fig. 3b). The dotted lines indicate the two unidirectional solutions, $x_1 = 1 - [1 + (\delta - \beta_0)^2]/g_0$ and $x_2 = 0$ (on the left), and $x_2 = 1 - [1 + (\delta + \beta_0)^2]/g_0$ and $x_1 = 0$ (on the right). We observe that the asymmetric bidirectional solution exists only for certain values of δ and β_0. In Figure 3a it exists for $-1.45 < \delta < 1.45$, as a transition between the symmetric bidirectional solution (for $\delta = 0$) and the unidirectional solution (for $|\delta| > 1.45$).

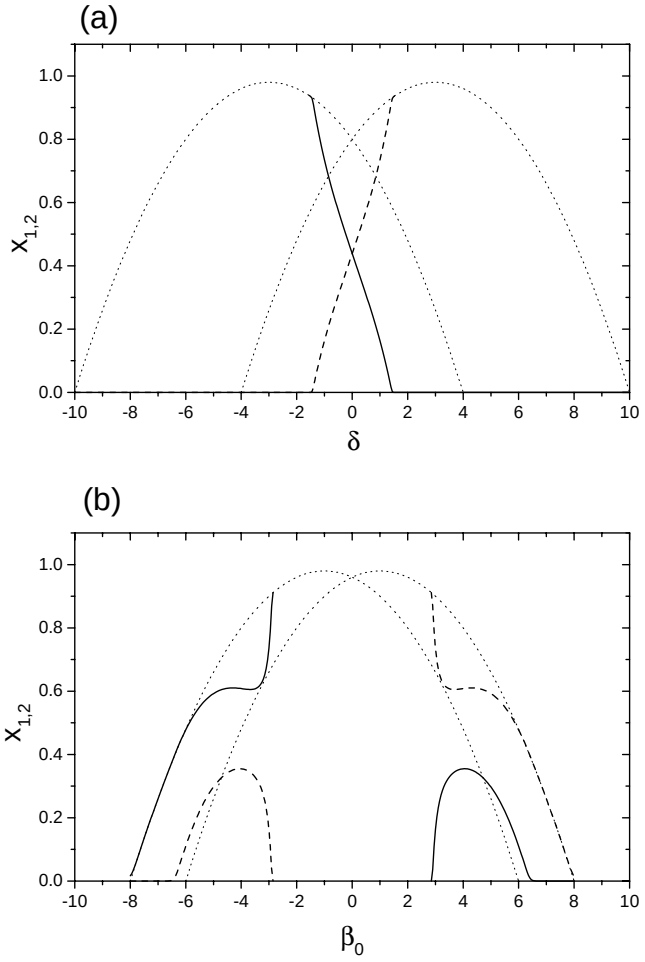

Fig. 3. Stationary asymmetric bidirectional solution for homogeneous broadening and $g_0 = 50$: x_1 (continuous line) and x_2 (dashed line) (a) *vs.* δ for $\beta_0 = -3$ and (b) *vs.* β_0 for $\delta = -1$; dotted lines: unidirectional solutions $x_{1,2} = 1 - [1 + (\delta \mp \beta_0)^2]/g_0$.

In Figure 3b the asymmetric bidirectional solution exists between $|\beta_0| = 2.85$ and the laser threshold, $|\beta_0| = 8$, for which $x_{1,2} = 0$.

For inhomogeneous broadening, the case $\delta = 0$ and $\beta_0 = 0$ is of particular interest, as it refers to a case of pure thermal motion, with no drift due to recoil. Moreover, we have seen above that in this case the symmetric bidirectional solution is also a possible stationary solution. Figure 4a shows the mode amplitudes x_1 (continuous line) and x_2 (dashed line) as a function of σ, for $g_0 = 50$, $\delta = 0$ and $\beta_0 = 0$. For $\sigma = 0$, $x_2 = 0$ and the solution is unidirectional. Increasing σ, the previously suppressed mode x_2 grows until it reaches the same level as the mode x_1 and the solution becomes symmetric. Figure 4b shows x_1 and x_2 as functions of β_0 for $\delta = 0$, $\sigma = 3$ and $g_0 = 50$. We observe that increasing β_0, the asymmetric bidirectional solution eventually becomes symmetric, with $x_1 = x_2$ when $|\beta_0| > 4.5$.

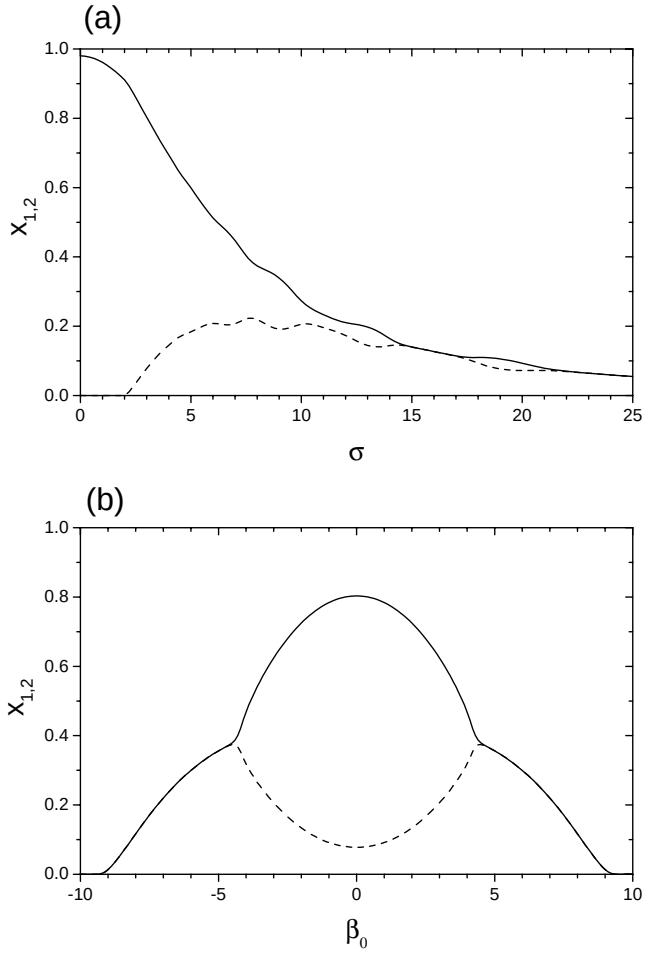

Fig. 4. Stationary asymmetric bidirectional solution for inhomogeneous broadening with Gaussian velocity distribution, $g_0 = 50$ and $\delta = 0$: x_1 (continuous line) and x_2 (dashed line) (a) *vs.* σ for $\beta_0 = 0$ and (b) *vs.* β_0 for $\sigma = 3$.

6 Stability analysis

6.1 Stability of the unidirectional solution

In order to investigate the stability of the unidirectional solution for uniform atomic motion, we linearise equation (36) assuming $x_1 = x_{10} + \epsilon_1(\tau)$ and $x_2 = \epsilon_2(\tau)$, where $\epsilon_{1,2}$ are small, time-dependent quantities and x_{10} is the stationary unidirectional solution. Expanding the r.h.s. of equation (36) up to the first power of ϵ_1 and ϵ_2, a straightforward calculation yields

$$\frac{\mathrm{d}\epsilon_1}{\mathrm{d}\tau} = -x_{10}\int \mathrm{d}\beta \frac{g_1^2 f(\beta)}{(1+g_1x_{10})^2} \times \left\{\epsilon_1 + \left[(1+g_1x_{10})\left(\mathrm{Re}C_1 - \delta_1 \mathrm{Im}C_1\right) + \left(\frac{1+\delta_1^2}{1+\delta_2^2} - 2g_1x_{10}\mathrm{Re}C_2\right)\right]\epsilon_2\right\}$$

$$\frac{\mathrm{d}\epsilon_2}{\mathrm{d}\tau} = \left\{-1 + \int \mathrm{d}\beta \frac{g_1 f(\beta)}{1+g_1x_{10}}\left(\frac{1+\delta_1^2}{1+\delta_2^2}\right) \times \left[1 - g_1x_{10}\left(\mathrm{Re}C_1 + \delta_2 \mathrm{Im}C_1\right)\right]\right\}\epsilon_2$$

where

$$C_1 = \frac{\mathcal{L}_{1,0}}{1 + \mathrm{i}2\gamma\beta + g_1x_{10}\mathcal{L}_{1,-1}}$$

and $C_2 = \mathcal{L}_{1,0}C_1$. The two eigenvalues of the linear problem are

$$\lambda_1 = -x_{10}\int \mathrm{d}\beta \frac{g_1^2 f(\beta)}{(1+g_1x_{10})^2} \tag{50}$$

and

$$\lambda_2 = -1 + \int \mathrm{d}\beta \frac{g_1 f(\beta)}{1+g_1x_{10}}\left(\frac{1+\delta_1^2}{1+\delta_2^2}\right) \times \left[1 - g_1x_{10}\left(\mathrm{Re}C_1 + \delta_2 \mathrm{Im}C_1\right)\right]. \tag{51}$$

The unidirectional solution is stable if both the eigenvalues are negative, whereas it is unstable if at least one eigenvalue is positive. From (50) and (51), it can be shown that λ_1 is always negative, whereas λ_2 can be positive for appropriate values of δ, β_0 and σ. We observe that λ_2 is invariant under the sign inversion of both δ and β_0 and in particular is symmetric with respect to β_0 when $\delta = 0$. Figures 5a and 5b show contour lines of λ_2, for homogeneous broadening, (a) as a function of mean atomic velocity, β_0, and atom-field detuning, δ, for a case of high-gain ($g_0 = 50$), and (b) as a function of β_0 and gain g_0 when $\delta = 0$. Here and in all the cases below, we assume, where not explicitly stated, that $\gamma = 1$. The dark gray regions in Figure 5 correspond to regions where the laser is below threshold ($g_1 < 1$) and the unidirectional solution does not exist. The light gray color indicates the region where λ_2 is negative, *i.e.* the unidirectional solution with $x_2 = 0$ is stable. The stability of the other unidirectional solution, with $x_1 = 0$, can be obtained from Figure 5 by changing the sign of δ. What can be deduced from Figure 5a is that for $\beta_0 = 0$ (atoms at rest) the unidirectional solution is stable for all values of the atom-field detuning δ. Increasing β_0, one or both of the unidirectional solutions become unstable for β_0 larger than a definite threshold value, which depends on δ and the gain g_0. At resonance ($\delta = 0$) the two unidirectional solutions are both unstable for $|\beta_0|$ larger than the threshold value, independently of the direction of the atomic motion. For positive (negative) detuning, the instability rate is larger for the mode propagating parallel (anti-parallel) to the atomic beam. We note that for a sufficiently large value of δ one of the two unidirectional solutions is stable, as may be observed in Figure 5a. This suggests a natural method to obtain truly unidirectional operation, with the laser emitting in one direction independent of the initial conditions.

$$\lambda_2 = -(g_1-1)\left\{\frac{(1+9\beta_0^2)[1-(1+4\gamma)\beta_0^2+(g_1-1)(1+\beta_0^2)(1+7\beta_0^2)]}{[1+9\beta_0^2+(g_1-1)(1+5\beta_0^2)]^2+4\beta_0^2[\gamma(1+9\beta_0^2)-(g_1-1)(1+3\beta_0^2)]^2}\right\}, \tag{52}$$

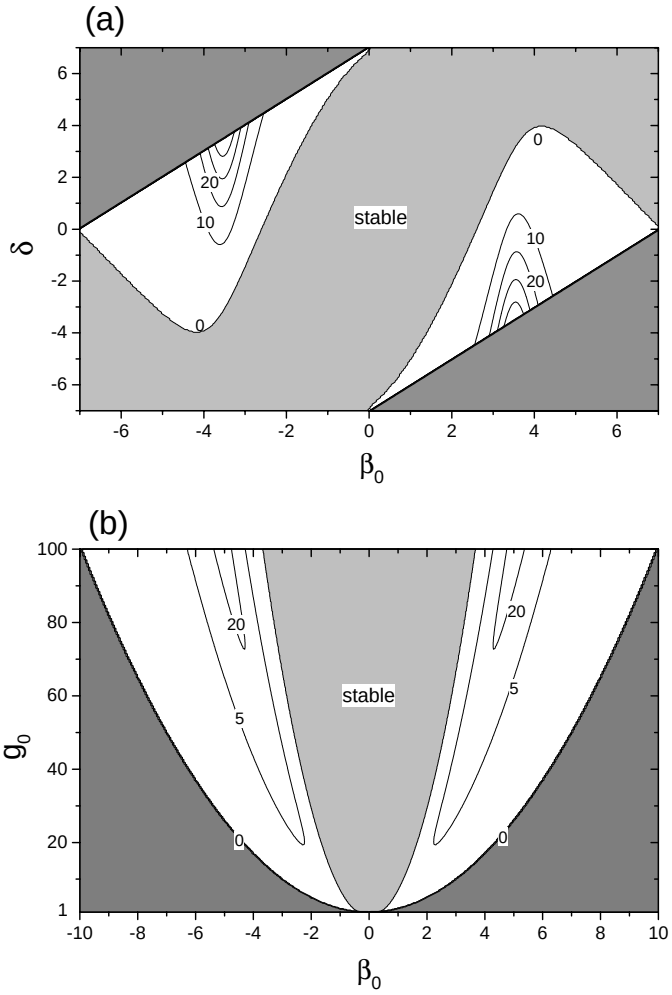

Fig. 5. Contour plot of the instability rate λ_2 of the unidirectional solution in a homogeneously broadened ring laser, (a) as a function of β_0 and δ for $g_0 = 50$ and (b) as a function of β_0 and g_0 for $\delta = 0$.

The eigenvalue λ_2 may be calculated explicitly for the resonant case $\delta = 0$ and for a homogeneously broadened medium as:

see equation (52) above,

where now $g_1 = g_0/(1+\beta_0^2)$. We note that for $\beta_0 = 0$ (atoms at rest), $\lambda_2 = -(g_1-1)/g_1$ and the unidirectional solution is stable. Near the laser threshold, $g_1 \approx 1$, the unidirectional solution is unstable for $\beta_0 > 1/\sqrt{1+4\gamma}$, whereas when $\gamma = 1$ it is unstable for

$$\frac{7g_0 - 4 + \sqrt{16+152g_0+49g_0^2}}{104} < \beta_0^2 < g_0 - 1, \tag{53}$$

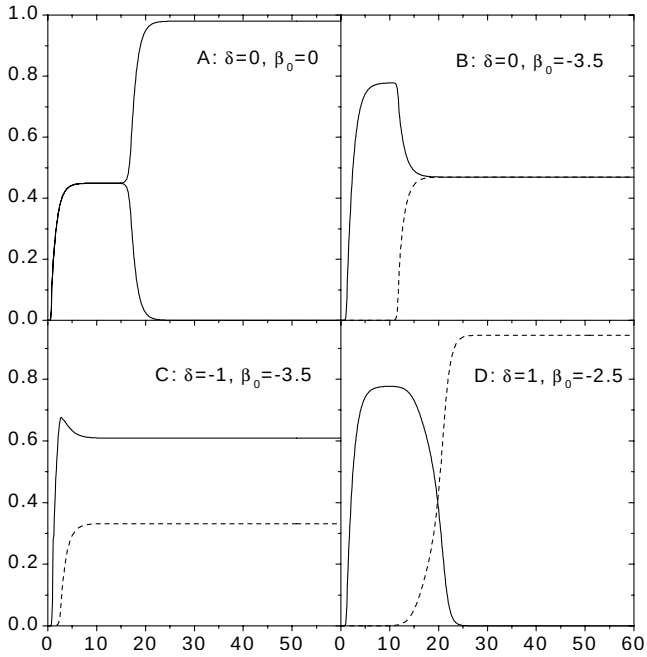

Fig. 6. Evolution of x_1 (continuous line) and x_2 (dashed line) *vs.* τ in a homogeneously broadened ring laser, for $g_0 = 50$ and different values of δ and β_0. A: $\delta = 0$ and $\beta_0 = 0$; B: $\delta = 0$ and $\beta_0 = -3.5$; C: $\delta = -1$ and $\beta_0 = -3.5$; D: $\delta = 1$ and $\beta_0 = -2.5$.

as shown in Figure 5b. For large g_0, the threshold value of the mean atomic velocity is $\beta_0 \approx 0.37\sqrt{g_0}$.

When the unidirectional solution with $x_2 = 0$ is unstable, the laser evolves towards a different stationary solution, *i.e.* the symmetric bidirectional solution when $\delta = 0$ or the asymmetric bidirectional solution or unidirectional solution with $x_1 = 0$ when $\delta > 0$. Figure 6 shows the evolution of x_1 (continuous line) and x_2 (dashed line) as a function of τ for homogeneous broadending, $g_0 = 50$ and different values of atom-field detuning, δ, and mean atomic velocity, β_0. The results are obtained by integrating equations (1–7) when the effects of recoil are artificially "switched off" by setting $\mathrm{d}\beta/\mathrm{d}t = 0$ and $\beta(0) = \beta_0$ constant. As a physical example of parameters, we assumed a sodium sample with resonant wavelength $\lambda = 589$ nm, $\mu = 10^{-29}$ C m, $\gamma_\perp = \gamma_\parallel = 10\kappa_c = 10^8$ s^{-1}, $D^{eq} = 1/2$ and $n = 6\times10^8$ cm^{-3}. In A, $\delta = 0$, $\beta_0 = 0$ and the initial field intensity are $x_1(0) = x_2(0) + 10^{-22}$ and $x_2(0) = 10^{-6}$: the symmetric bidirectional solution is unstable, whereas the unidirectional solution with $x_2 = 0$ is stable. We note that, since the ring laser has no preferred direction, it can oscillate in either of the modes as determined by initial fluctuations. In B, the atoms are now moving in the negative-z direction ($\beta_0 = -3.5$), and $\delta = 0$, $x_1(0) = 10^{-6}$ and $x_2(0) = 10^{-58}$: in this case the unidirectional solution

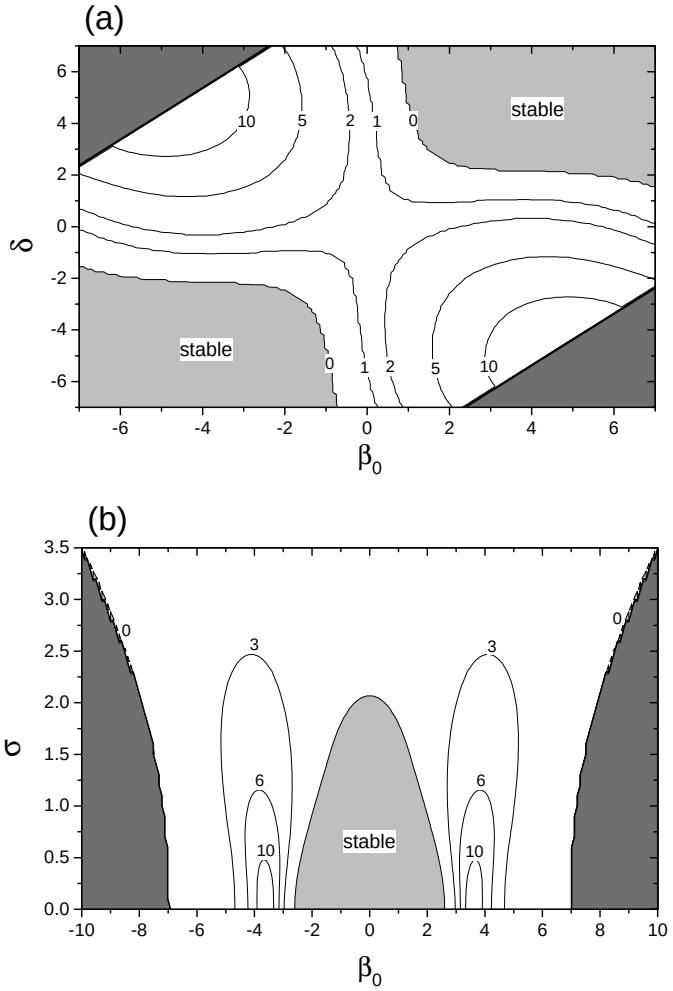

Fig. 7. Contour plot of the instability rate λ_2 of the unidirectional solution in an inhomogeneously broadened ring laser with Gaussian velocity distribution and $g_0 = 50$, (a) as a function of β_0 and δ for $\sigma = 3$, and (b) as a function of β_0 and σ for $\delta = 0$.

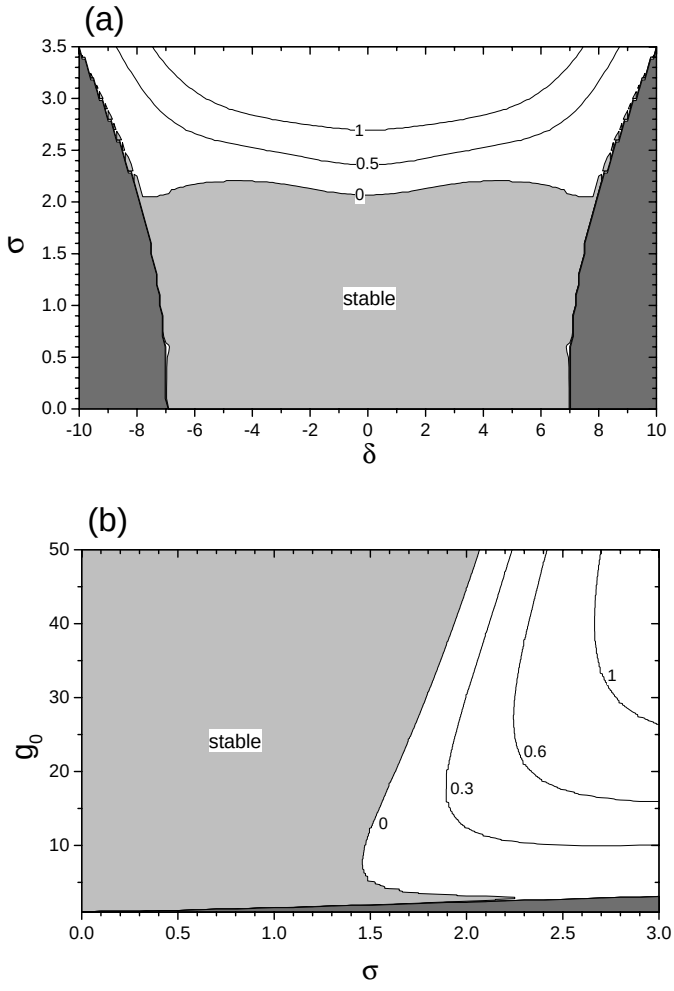

Fig. 8. Contour plot of the instability rate λ_2 of the unidirectional solution in an inhomogeneously broadened ring laser with Gaussian velocity distribution and $\beta_0 = 0$, (a) as a function of δ and σ for $g_0 = 50$ and (b) as a function of σ and g_0 for $\delta = 0$.

is unstable whereas the symmetric bidirectional solution is stable. Different behaviors occur when the laser is detuned. In C, $\delta = -1$, $\beta_0 = -3.5$ and $x_1(0) = x_2(0) = 10^{-6}$: the gain rates g_1 and g_2 are different and the two modes saturate at different levels (asymmetric bidirectional solution). In D, $\delta = 1$, $\beta_0 = -2.5$, $x_1(0) = 10^{-6}$, and $x_2(0) = 10^{-22}$: due to a larger initial seed, the mode x_1 saturates before the mode x_2. However, the unidirectional solution with $x_2 = 0$ is unstable, whereas that with $x_1 = 0$ is stable, so a mode exchange occurs.

Figure 7 shows that inhomogenoues broadening significantly modifies the stability of the unidirectional solution. Figures 7a and 7b show the contour lines of λ_2, for inhomogeneous broadening and $g_0 = 50$, (a) as a function of β_0 and δ when $\sigma = 3$ and (b) as a function of β_0 and σ when $\delta = 0$. As before, the dark gray color corresponds to the laser below threshold and the light gray color to the stability of the unidirectional solution with $x_2 = 0$. Figures 8a and 8b show the contour lines of λ_2, for inhomogeneous broadening and stationary atoms ($\beta_0 = 0$) (a) as a function of δ and σ for $g_0 = 50$, and (b) as a function of σ and g_0 when $\delta = 0$. We observe, from Figures 7 and 8, that the unidirectional solution is unstable for stationary atoms (with $\beta_0 = 0$) for any detuning when the velocity spread σ exceeds a threshold value which depends on g_0. Hence thermal motion, causing Doppler broadening, destabilizes the unidirectional solution, which is stable for cold atoms ($\sigma = 0$). For the case of Figure 7a, the unidirectional solution is stable only for sufficiently large values of δ and β_0 with the same sign.

Figure 9 shows the evolution of x_1 (continuous line) and x_2 (dashed line) as a function of τ in a case of inhomogeneous broadening with $g_0 = 50$ and $\sigma = 3$, for different values of δ and β_0. The results have been obtained integrating numerically equations (1–7) with the recoil artificially "switched off", for the same parameters of Figure 6 and the atomic velocities distributed with a Gaussian weight around β_0 with $\sigma_v = 28.12$ m/s, corresponding to a temperature of 2.18 K. In A and B, $\delta = 0$, $\beta_0 = 0$ (Fig. 9A) and $\beta_0 = -2.5$ (Fig. 9B),

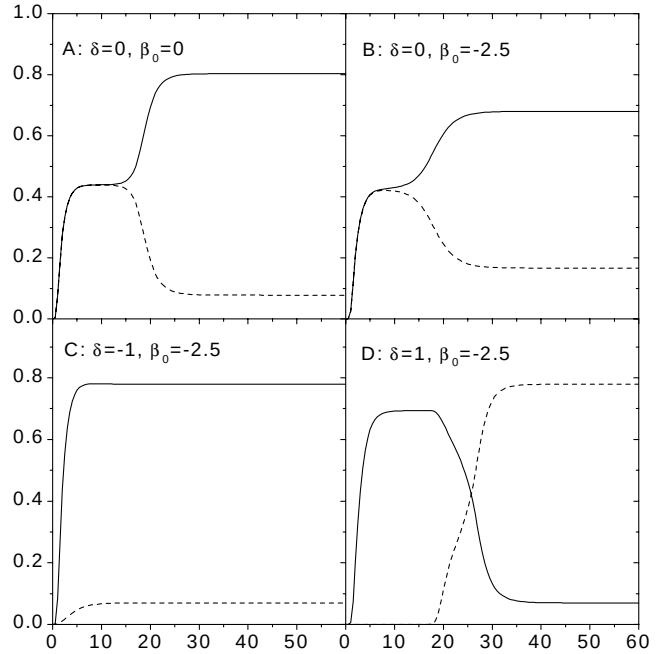

Fig. 9. Evolution of x_1 (continuous line) and x_2 (dashed line) *vs.* τ in an inhomogeneously broadened ring laser with Gaussian velocity distribution, for $g_0 = 50$, $\sigma = 3$ and different values of δ and β_0. A: $\delta = 0$ and $\beta_0 = 0$; B: $\delta = 0$ and $\beta_0 = -2.5$; C: $\delta = -1$ and $\beta_0 = -2.5$; D: $\delta = 1$ and $\beta_0 = -2.5$.

$x_1(0) = x_2(0) + 10^{-9}$ and $x_2(0) = 10^{-6}$: as in the homogeneous case, the symmetric bidirectional solution is unstable. However, now the stable solution is the asymmetric bidirectional solution and not the unidirectional solution. In a similar way, in Figures 9C and 9D, where $\delta = -1$, $\beta_0 = -2.5$, $x_1(0) = x_2(0) = 10^{-6}$ (Fig. 9C) and $\delta = 1$, $\beta_0 = -2.5$, $x_1(0) = 10^{-6}$ and $x_2(0) = 10^{-38}$ (Fig. 9D), the system evolves toward asymmetric bidirectional solutions, although with different gains. We note the existence, also in absence of coherent motion due to recoil (*i.e.* for $\beta_0 = 0$), of a asymmetric bidirectional emission in a inhomogeneously broadened ring laser. Similar results have been recently shown in a ring resonator driven by an external field and containing a saturable, homogeneously broadened absorber [26].

We note that Figures 6 and 9 have been obtained integrating numerically the exact equations (1–7) for uniform atomic motion and a set of physical parameters giving $g_0 = 50$, $\sigma = 0$ and $\sigma = 3$, respectively. However, the same results can be reproduced satisfactorly by solving numerically the reduced equation (36) for assigned values of β_0 and σ and neglecting the phase shifts $\Omega_{1,2}$. This confirms the validity of the approximations used in Section 4, where the Fourier components of the two polarisations and the population difference were eliminated adiabatically in the good cavity limit, $\kappa_c \ll \gamma_\perp, \gamma_\parallel$.

6.2 Stability of the symmetric bidirectional solution

We now investigate the stability of the symmetric bidirectional solution, restricting the analysis to the resonant case ($\delta = 0$). The symmetric bidirectional solution for a homogeneously broadened ($\sigma = 0$), detuned ($\delta \neq 0$) and stationary ($\beta_0 = 0$) medium is unstable, as demonstrated in Appendix B.

Defining $x_\pm = (x_1 \pm x_2)/2$ and setting $\delta = 0$, equations (36) can be recast in the following form

$$\frac{\mathrm{d}x_+}{\mathrm{d}\tau} + x_+ = \int \mathrm{d}\beta f(\beta) g_1 \frac{x_+ + \sqrt{x_+^2 - x_-^2}\, Z}{1 + 2g_1(x_+ + \sqrt{x_+^2 - x_-^2}\, Z)} \quad (54)$$

$$\frac{\mathrm{d}x_-}{\mathrm{d}\tau} + x_- = \int \mathrm{d}\beta f(\beta) g_1 \frac{x_-}{1 + 2g_1(x_+ + \sqrt{x_+^2 - x_-^2}\, Z)}, \quad (55)$$

where now $g_1 = g_0/(1+\beta^2)$ and $Z = \mathrm{Re}z_0 + \beta \mathrm{Im}z_0$. We linearise equations (54) and (55) assuming $x_+ = x_0 + \epsilon_+(\tau)$ and $x_- = \epsilon_-(\tau)$, where x_0 is the symmetric bidirectional solution, satisfying equation (46), and $\epsilon_\pm$ are small time-dependent quantities. It is possible to show, from equations (25, 26, 31), that the linear term of the expansion of z_0 as powers of ϵ_+ and ϵ_- contains only contributions proportional to ϵ_+. Hence, writing $Z = Z_0 + C_0\epsilon_+$, where Z_0 is the zeroth-order term, and expanding equations (54) and (55) up to first order in ϵ_+ and ϵ_-, we obtain

$$\frac{\mathrm{d}\epsilon_+}{\mathrm{d}\tau} = x_0 \left\{ \int \mathrm{d}\beta f(\beta) \frac{g_1[C_0 - 2g_1(1+Z_0)^2]}{[1 + 2g_1 x_0(1+Z_0)]^2} \right\} \epsilon_+ \equiv \lambda_+ \epsilon_+ \quad (56)$$

$$\frac{\mathrm{d}\epsilon_-}{\mathrm{d}\tau} = -\left\{ \int \mathrm{d}\beta f(\beta) \frac{g_1 Z_0}{1 + 2g_1 x_0(1+Z_0)} \right\} \epsilon_- \equiv \lambda_- \epsilon_-. \quad (57)$$

The coefficient C_0 in equation (56) is evaluated in Appendix C as an infinite series. For a homogeneously broadened medium, the two eigenvalues λ_+ and λ_- simplify to:

$$\lambda_+ = x_0[g_1 C_0(1 - 2x_0)^2 - 1] \quad (58)$$

$$\lambda_- = g_1(1 - 2x_0) - 1, \quad (59)$$

where we have used, from equation (47), the identity $(1 + Z_0)^{-1} = g_1(1 - 2x_0)$. The stability of the symmetric bidirectional solution for homogeneous broadening is shown in Figure 10a, where the contour lines of λ_- are plotted *vs.* β_0 and g_0. A numerical calculation of the constant C_0 shows that the eigenvalue λ_+ has the same sign as λ_-, so that a negative value of λ_- is a sufficient indication of stability of the bidirectional solution. The light gray color indicates a positive value of the eigenvalue, *i.e.* that the symmetric bidirectional solution is unstable. The stability region is limited by the above-threshold condition, $g_0 > 1 + \beta^2$, which guarantees the existence of the stationary solution, whereas the dark grey color indicates that the laser is below threshold. We observe that the instability region of the unidirectional solution, shown in Figure 5b, matches the stability region of the symmetric bidirectional solution of Figure 10a. It is interesting to note the existence of two regions (near $\beta_0 = \pm 2.5$) where the symmetric bidirectional solution and the unidirectional solution are both stable. It may correspond to a region of bistability where two equilibria coexists,

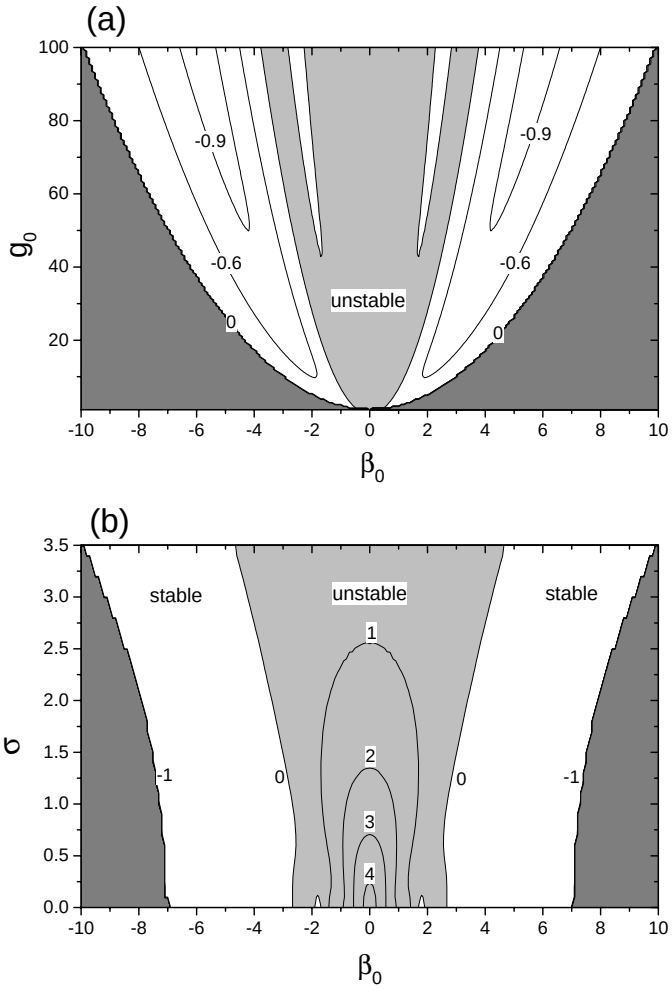

Fig. 10. Contour plot of the instability rate λ_- of the symmetric bidirectional solution and $\delta = 0$. (a): λ_- *vs.* β_0 and g_0 in a homogeneously broadened ring laser; (b): λ_- *vs.* β_0 and σ for $g_0 = 50$ in an inhomogeneously broadened ring laser.

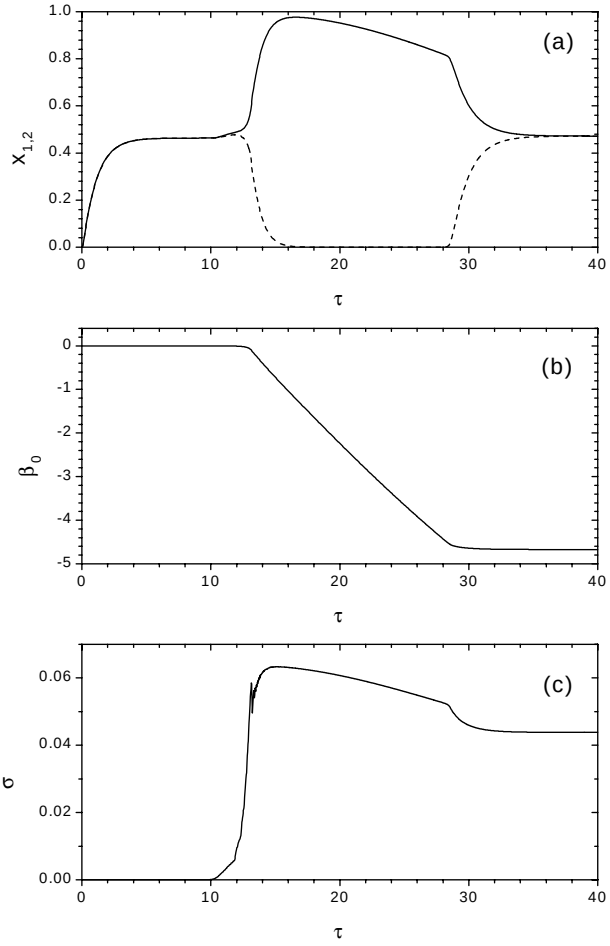

Fig. 11. Self-consistent dynamics with recoil in a resonant homogeneously broadened ring laser with $\delta = 0$, $g_0 = 50$ and $\tau_r = 3.2$, as obtained solving the exact equations (1–7); (a) x_1 (continuous line) and x_2 (dashed line), (b) β_0, and (c) σ, as a function of τ.

as has been verified by numerical integration of the time-dependent equations. Finally, Figure 10b shows the contour lines of λ_- as a function of β_0 and σ when $g_0 = 50$. Increasing σ, the instability region of the symmetric bidirectional solution around $\beta_0 = 0$ increases. Hence, for increasing inhomogeneous broadening an increasingly larger value of β_0 is necessary in order to stabilize the symmetric bidirectional solution.

7 Dynamics with recoil

We discuss now the numerical solution of equations (1–7) including recoil, for a gas of initially inverted, $D(0) = D^{\rm eq} = 1/2$, unpolarized, $S_1(0) = S_2(0) = 0$, and unbunched atoms (*i.e.* with $\theta(0)$ uniformly distributed over 2π). Furthermore, we assume that the atomic velocities are initially zero, $\beta(0) = 0$ (for a homogeneously broadened ring laser) or normally distributed around $\langle\beta(0)\rangle = 0$ (for an inhomogeneously broadened ring laser). The parameters of the simulations are close to these of a sodium vapor, with resonant wavelength $\lambda = 589$ nm, $\mu = 10^{-29}$ C m, $\gamma_\perp = \gamma_\parallel = 6.2 \times 10^7$ s^{-1}, $\kappa_c = 1.24 \times 10^5$ s^{-1}, $\omega_r = 6.2 \times 10^5$ s^{-1}, $L_s = 1$ cm, $L_{cav} = 1$ m and $n_s = 10^8$ cm^{-3}. The derived parameters are $g_0 = 50$ and $\tau_r = 3.2$.

7.1 Homogeneously broadened ring laser

Figure 11a shows x_1 (continuous line) and x_2 (dashed line), as a function of τ when the atoms are allowed to recoil under the influence of the cavity modes. The gas is initially cold, at rest and in resonance, with $f(\beta) = \delta(\beta)$ and $\delta = 0$. The initial intensities are $x_1(0) = x_2(0) + 10^{-20}$ and $x_2(0) = 10^{-4}$. Figures 11b and 11c show the evolution of β_0 and σ as functions of τ. The results agree with those of Figures 6A and 6B: initially $x_1 = x_2$ and $\beta_0 = 0$, in agreement with equation (38). As shown by the linear analysis, for $\beta_0 = 0$ the symmetric bidirectional solution is unstable and the unidirectional solution is stable, so that the mode x_2 is suppressed and x_1 reaches a saturation value close to one. However, the unbalanced

radiation pressure for $x_1 \gg x_2$ drives the atoms anti-parallel to the mode x_1, with the average velocity decreasing as $\beta_0 \approx -\tau/\tau_r$. When β_0 reaches the threshold value of -2.6, given by equation (53), the unidirectional solution becomes unstable and the bidirectional solution stable. Finally, β_0 reaches the stationary value -4.7 when $x_1 = x_2$. We note, from Figure 11c, that σ remains much smaller than one, so that the inhomogeneous broadening effects are negligible.

A simple intuitive interpretation of this result may be given in terms of the Doppler shift due to the longitudinal momentum induced by radiation pressure. An atom moving with an axial velocity v_z effectively sees two different Doppler-shifted frequencies $\omega'_{1,2} = \omega(1 \mp v_z/c)$. The atom is resonant with the radiation when these shifted frequencies coincide with the atomic resonance, that is, when $\omega_0 = \omega(1 \mp \langle v_z \rangle/c)$. Consequently, for atomic velocities sufficiently large, two modes with equal frequencies in the laboratory frame may be widely separated in frequency in the rest frame of the atom. When $\omega_0 = \omega$, *i.e.* $\delta = 0$, x_1 and x_2 are shifted from resonance by the same amount but in different directions, and hence experience equal gains $g_1 = g_2$. The separation between the two line centers reduces the influence of one mode on the other, making the two modes effectively uncoupled. This occurs approximately when the frequency difference between the line centers, $k|\langle v \rangle_z|$, exceeds the gain linewidth, $\gamma_\perp$. In fact, we observe from Figure 11a that x_1 starts to decrease when $\beta_0 \approx -1$, *i.e.* $k|\langle v \rangle_z| \sim \gamma_\perp$. This occurs in a time $\tau \sim \tau_r$, *i.e.* in a typical time of the order of the inverse of the recoil frequency ω_r.

Figure 12 shows the evolution of x_1 and x_2, (a), β_0, (b), and σ, (c), for a blue-detuned case, $\delta = 1$, and the same other parameters as in Figure 11. Initially, when $\beta_0 = 0$, the symmetric bidirectional solution is unstable and the two unidirectional solutions are stable. As in the previous case of Figure 11a, the laser evolves toward the unidirectional solution with $x_2 = 0$, and β_0 becomes negative, with the atoms moving anti-parallel to the field x_1. When β_0 reaches the value -2.2 for which the unidirectional solution is unstable, the mode x_1 decays and the mode x_2 grows up to saturation in a way similar to the case of Figure 6D; successively, β_0 reaches a minimum when $x_1 = x_2$ and then increases until it becomes positive and reaches the instability threshold for the mode x_1, $\beta_0 = 2.2$. Then, x_2 decays to zero and x_1 grows again to saturation. This process continues periodically, with the modes growing alternately toward saturation and then decaying. In this case, the unbalanced radiation pressure induces a mean atomic velocity which Doppler-shifts the frequency of the mode whose intensity is lower toward resonance, pushing the other (more intense) mode further away from resonance. The role of the two modes is exchanged when one intensity exceeds the other, and β_0 changes sign. The growing mode reaches the maximum when its effective frequency is resonant with the atoms, *i.e.* when $|\beta_0| \approx \delta$: as shown by Figure 12a, x_1 and x_2 are maxima when $\beta_0 \sim \mp 1$, respectively.

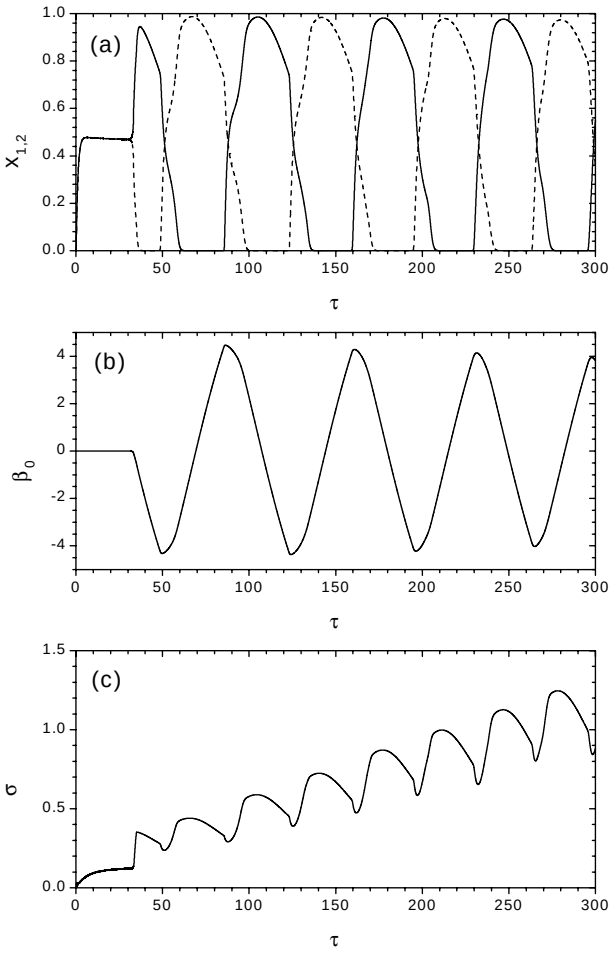

Fig. 12. Self-consistent dynamics with recoil in a blue-detuned homogeneously broadened ring laser with $\delta = 1$ and the other parameters as in Figure 11; (a) x_1 (continuous line) and x_2 (dashed line), (b) β_0 and (c) σ, as a function of τ.

Figure 13a shows the behavior of the intensities of the two modes for a red-detuned case, with $\delta = -1$ and the other parameters as in Figure 11. As in Figure 11a, the symmetric bidirectional solution is unstable when $\beta_0 = 0$, and the laser evolves toward the unidirectional solution with $x_2 = 0$. Then, β_0 becomes negative, until eventually it is less than -3 and the unidirectional solution is unstable (see Fig. 5a for $\delta = -1$ and β_0 negative). As shown by Figure 6C, the stable solution in this case is the asymmetric bidirectional solution with both x_1 and x_2 different from zero. Because $x_1 > x_2$, β_0 continues to decreases until $g_{1,2} < 1$, which occurs for $\beta_0 < -8$ and $\beta_0 < -6$, respectively. Hence, in the red-detuned case ($\delta < 0$) the unbalanced radiation pressure induces a mean atomic velocity which drives both modes below threshold.

7.2 Inhomogeneously broadened ring laser and self-cooling

Figure 14 shows the evolution of the resonant ($\delta = 0$) ring laser when the medium is initially Doppler broadened with

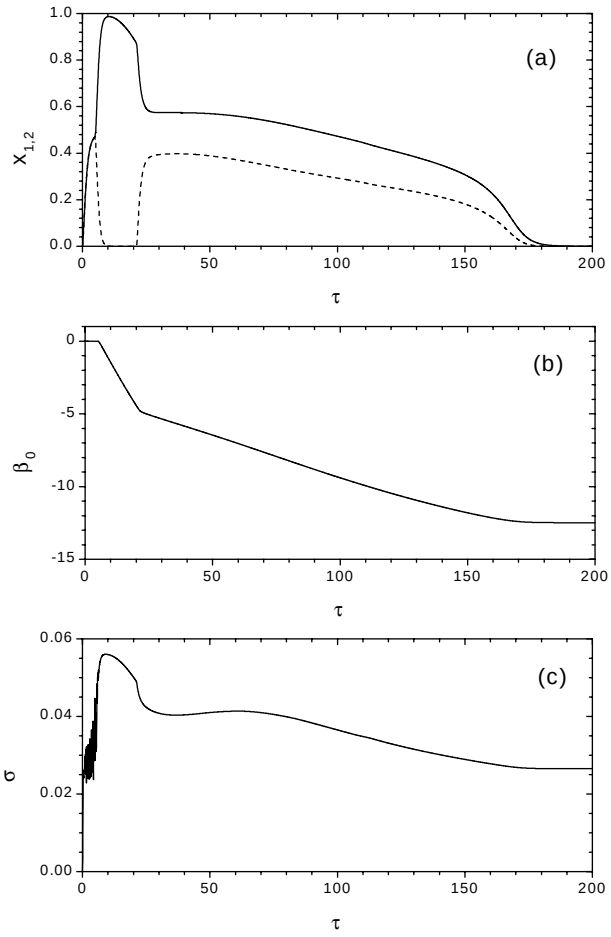

Fig. 13. Self-consistent dynamics with recoil in a red-detuned homogeneously broadened ring laser with $\delta = -1$ and the other parameters as in Figure 11; (a) x_1 (continuous line) and x_2 (dashed line), (b) β_0, and (c) σ, as a function of τ.

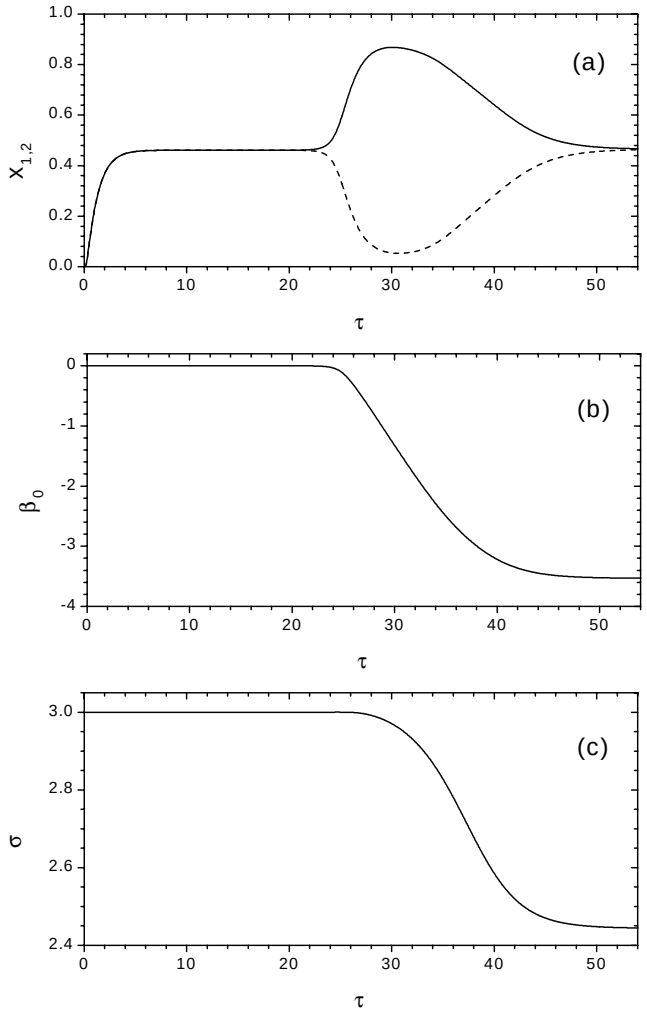

Fig. 14. Self-consistent dynamics with recoil in a resonant inhomogeneously broadened ring laser with Gaussian velocity distribution, with $\sigma(0) = 3$, $\delta = 0$ and the other parameters as in Figure 11; (a) x_1 (continuous line) and x_2 (dashed line), (b) β_0, and (c) σ, as a function of τ.

$\sigma = 3$. The other parameters are the same as in Figure 11. The two modes behave in a way similar to the homogeneous broadened case, with the symmetric bidirectional solution initially unstable when $\beta_0 = 0$ and successively stable when the atoms move antiparallel to the mode x_1 with $\beta_0 = -2.3$. The stability analysis (see Fig. 10b) shows that for $\sigma = 3$ and $|\beta_0| < 4.5$ the symmetric bidirectional solution is unstable, and Figures 9A and 9B show that neglecting recoil the laser evolves toward the asymmetric bidirectional solution with $x_1 > x_2$. However, the decrease of σ, shown in Figure 14c, lowers the stability threshold for β_0, as shown by Figure 10b, so that for the stationary values of $\sigma = 2.45$ and $\beta_0 = -3.5$ the symmetric solution with $x_1 = x_2$ is stable. The slight decrease of σ during the unidirectional emission is an interesting example of atomic self-cooling, where the temperature of the atomic medium decreases spontaneously during the lasing. A similar effect was recently predicted in a passive (*i.e.* non-inverted) collection of atoms with a finite velocity spread and driven by an external laser beam [10]. A small probe can be exponentially amplified *via* population difference grating effects to a saturated value almost equal to that of the pump. In this saturated regime the width of the velocity distribution of the atomic sample decreases significatively. Here, we observe a rather different effect, where the width σ of the velocity distribution decreases due to the effect of a single field. Although the narrowing of the velocity distribution curve is only about 20% in the resonant case of Figure 14c, a more effective self-cooling is observed when the laser is blue-detuned, as shown in Figure 15 for $\delta = 1$ and the same other parameters as in Figure 14.

The principle at the base of the observed effect is the same as that of optical molasses [27], in which two weak counter-propagating laser beams are used to cool of a collection of non-inverted atoms. The total force on an atom can be written as the sum of the radiation pressure from each of the two beams, resulting in a damping force $F(v) = -\alpha v$ when the laser frequency is red-detuned with respect to the atomic resonance. The same effect has been demonstrated using two strong counter-propagating laser beams alternated in time [28], with 50% duty factor and the duration of each beam longer than the

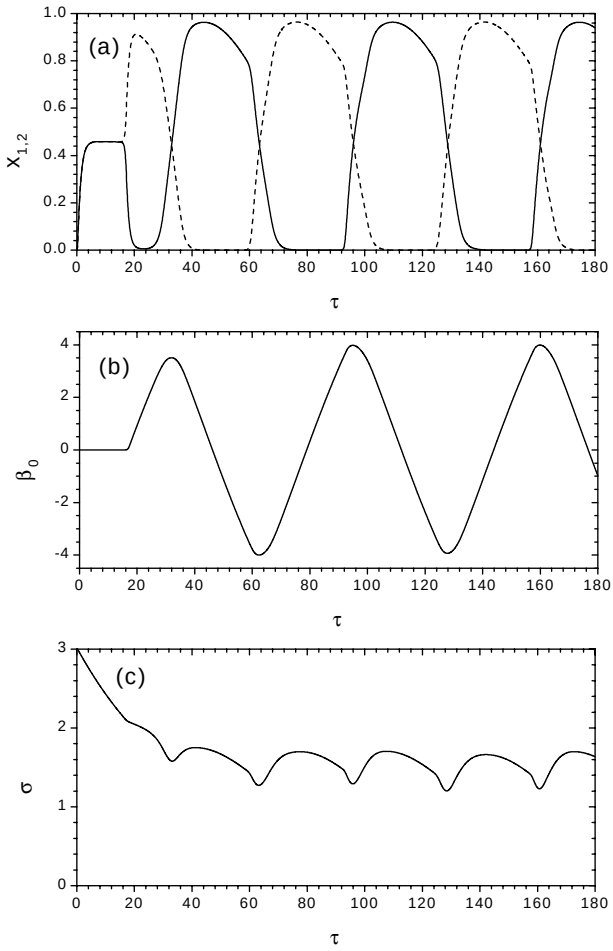

Fig. 15. Self-consistent dynamics with recoil in a blue-detuned inhomogeneously broadened ring laser with Gaussian velocity distribution, $\sigma(0) = 3$, $\delta = 1$ and the other parameters as in Figure 11; (a) x_1 (continuous line) and x_2 (dashed line), (b) β_0, and (c) σ, as a function of τ.

atomic relaxation time $\gamma_\parallel^{-1}$ and shorter than the damping time M/α, where M is the atomic mass. We describe here a different situation, where the direction of the fields is "switched" by the atoms themselves. Furthermore, it is not necessary to chirp the frequency of the laser to mantain it in resonance with the atoms to decelerate, as, in our case, they are decelerated by their own emitted field.

It is possible to give an analytical description of the atomic self-cooling in the presence of unidirectional emission, with the mode x_1 (x_2) propagating along the positive (negative) direction of the z-axis, with $x_2 = 0$ ($x_1 = 0$). Assuming $x_{1,2}$ and $\Omega_{1,2}$ stationary and given by equations (41, 42) and their respective expressions for x_2 and Ω_2, equations (38) and (39) become:

$$\frac{\mathrm{d}\beta_0}{\mathrm{d}\tau} = \mp(x_{1,2}/\tau_\mathrm{r}) \tag{60}$$

$$\frac{\mathrm{d}}{\mathrm{d}\tau}\left[\sigma^2 + \beta_0^2\right] = \mp(2/\tau_\mathrm{r}) g_0 x_{1,2} \times \int \mathrm{d}\beta \frac{\beta f(\beta)}{1 + g_0 x_{1,2} + (\beta \mp \delta)^2}, \tag{61}$$

where the upper (lower) sign refers to x_1 (x_2). Changing the integration variable to $q = \beta - \beta_0$ and defining $f_0(q) = f(\beta_0 + q)$, equation (61) with the help of equations (41) and (60) becomes:

$$\frac{\mathrm{d}\sigma^2}{\mathrm{d}\tau} = -(2/\tau_\mathrm{r}) g_0 x \int \mathrm{d}q \frac{q f_0(q)}{\xi^2 + (q - \delta_0)^2}, \tag{62}$$

where $x = x_{1,2}$, $\xi = \sqrt{1 + g_0 x}$ and $\delta_0 = \delta \mp \beta_0$. A qualitative examination of equation (62) allows for a simple interpretation of the self-cooling mechanism. The function under the integral is the product of an antisymmetric function $q f_0(q)$, with a maximum at $q \sim \sigma$, and a Lorentzian of width ξ and center at $q = \delta_0$. The integral is positive (and therefore σ is decreasing) when the center of the Lorentzian lies on the positive axis of q, *i.e.* when $\delta > \pm\beta_0$. Because equation (60) indicates that β_0, initially zero, decreases (increases) in the presence of the mode x_1 (x_2), cooling always occurs when $\delta \geq 0$, whereas only for $|\beta_0| > |\delta|$ when $\delta < 0$. More important, the cooling occurs independently of which mode propagates within the cavity, as can be observed in Figure 15. When $\sigma \gg \xi$, the optimum detuning for a maximum rate of cooling is $\delta_0 \sim \sigma$.

In the case of a Gaussian distribution $f_0(q) = (1/\sigma\sqrt{2\pi}) \exp(-q^2/2\sigma^2)$, the integral of equation (62) can be expressed, using equation (45), in terms of error function of complex argument:

$$\frac{\mathrm{d}\sigma^2}{\mathrm{d}\tau} = -(2/\tau_\mathrm{r}) x \left[\delta_0 - \frac{g_0}{\sigma}\sqrt{\frac{\pi}{2}} \mathrm{Im}\, W\left(\frac{\delta_0 + \mathrm{i}\xi}{\sqrt{2}\sigma}\right)\right], \tag{63}$$

where $W(z) = \exp(-z^2)\mathrm{erfc}(-\mathrm{i}z)$. A relatively simple expression can be obtained assuming that the velocity distribution function has a Lorentzian shape, with $f_0(q) = (\sigma/\pi)/(\sigma^2 + q^2)$. In this case, the integrals in equations (62) and (41) can be explicitely evaluated giving,

$$\tau_\mathrm{r} \frac{\mathrm{d}\sigma}{\mathrm{d}\tau} = -\frac{\delta_0 x}{\xi + \sigma}, \tag{64}$$

where ξ is the solution of the cubic equation $g_0(\xi + \sigma) = \xi[\delta_0^2 + (\xi + \sigma)^2]$. We observe from equation (64) that, for $\delta_0 > 0$, σ decreases monotonically in the presence of either x_1 or x_2, in agreement with the previous discussion.

An approximate expression of the atomic self-cooling can be obtained for small values of σ: evaluating asymptotically the function $W(z)$ in equations (44) and (63), a straightforward calculation yields, for $\sigma \ll \sqrt{g_0}$:

$$\tau_\mathrm{r} \frac{\mathrm{d}\sigma}{\mathrm{d}\tau} = -\frac{2\delta_0 x}{g_0}\sigma, \tag{65}$$

so that

$$\sigma(\tau) = \sigma(0)\, \mathrm{e}^{-(2\delta_0 x/g_0)(\tau/\tau_\mathrm{r})}. \tag{66}$$

The opposite limit of large inhomogeneous broadening, $\sqrt{g_0} \ll \sigma < g_0$, can be obtained from equation (64) as

$$\tau_\mathrm{r} \frac{\mathrm{d}\sigma}{\mathrm{d}\tau} = -\frac{\delta_0 g_0 \sigma}{(\delta_0^2 + \sigma^2)^2}, \tag{67}$$

showing that in general the self-cooling is less efficient for initially large velocity spread. In particular, we observe that the r.h.s term of equation (67) presents a maximum of $-0.32 g_0/\sigma^2$ for the optimum detuning $\delta_0 = \sigma/\sqrt{3}$.

The results obtained neglect the influence of momentum diffusion due to spontaneous emission, which is responsible for the well-known Doppler-cooling limit [28]. In fact, atoms undergoing spontaneous emission emit photons in random directions. Consequently, the atoms feel randomly directed momentum "kicks" of magnitude $\hbar k$. The long term effect of this is to cause a random walk in momentum space. In an ideal one-dimensional situation, after N emissions, according to the usual random-walk theory, the mean square velocity is $\langle v^2 \rangle \approx N(\hbar k/M)^2 t = \rho_{bb}\gamma_\parallel(\hbar k/M)^2 t$ [29], as $N = \rho_{bb}\gamma_\parallel t$, where ρ_{bb} is the probability of finding an atom in the upper state $|b\rangle$. In the scaled notation of this paper,

$$\sigma^2_{\rm diff} \approx (\omega_{\rm r}/\gamma_\perp)\frac{1+\delta_0^2}{g_0}(\tau/\tau_{\rm r}), \tag{68}$$

where we have assumed saturation, $x \approx 1$, $\rho_{aa} \approx 0$, and $\rho_{bb} \approx D = D^{\rm eq}(1+\delta_0^2)/g_0$. Including the heating contribution due to momentum diffusion, equation (65) is modified as:

$$\tau_{\rm r}\frac{{\rm d}\sigma^2}{{\rm d}\tau} \approx -\frac{4\delta_0}{g_0}\sigma^2 + (\omega_{\rm r}/\gamma_\perp)\frac{1+\delta_0^2}{g_0}, \tag{69}$$

which shows that σ^2 tends asymptotically toward the limit

$$\sigma^2_{\rm Dop} = \frac{1+\delta_0^2}{4\delta_0}(\omega_{\rm r}/\gamma_\perp), \tag{70}$$

which minimizes for $\delta_0 = 1$, giving $\sigma^2_{\rm Dop} = \omega_{\rm r}/2\gamma_\perp$, *i.e.* the well-known Doppler-cooling limit $T_{\rm Dop} = \hbar\gamma_\perp/k_{\rm B}$.

Finally, we test the reduced model of equations (36–39), assuming the Gaussian distribution (40) for the atomic velocities. The result of the numerical integration of the reduced model for $g_0 = 50$, $\delta = 1$, $\tau_{\rm r} = 3.2$ and the same initial conditions as in Figure 15 is shown in Figure 16: we observe that the solution of the reduced model describes the solution of the exact equations (1–7) quite satisfactorly, both for the fields and the atomic motion, although the cooling shown in Figure 15 is less than that of Figure 16, perhaps because the real velocity distribution differs from the ideal Gaussian distribution assumed in the reduced model. Figure 17a shows histograms of the velocity distribution for the case of Figure 15, as obtained form the multi-particle simulations at $\tau = 0$ and $\tau = 60$. Finally, a numerical study has shown that self-cooling can be optimized with a suitable choice of the recoil time $\tau_{\rm r}$: Figure 17b reports the best result obtained for $\tau_{\rm r} = 2$ and the other parameters as in Figure 15. The continuous and dashed lines show σ *vs.* τ as obtained by numerical integration of the multi-particle model and of the reduced model, respectively. We observe a monotonic decrease of σ, from $\sigma = 3$ to $\sigma = 0.1$ after $\tau = 130$.

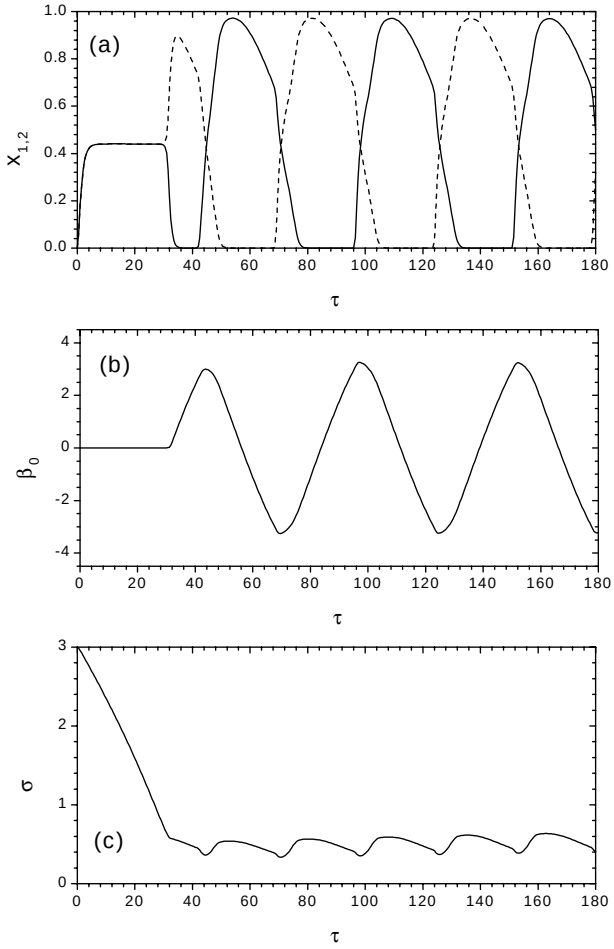

Fig. 16. Solution of the reduced equations (36–39), for the same parameters as in Figure 15; (a) x_1 (continuous line) and x_2 (dashed line), (b) β_0, and (c) σ, as a function of τ.

8 Discussion and conclusions

We complete the description of the effects of the atomic motion in a bidirectional ring laser with a short discussion of their possible observation in a realistic experiment. The main difficulty consists in finding an atomic vapor where population inversion can be created without destroying the coherent motion induced by recoil. For this reason, incoherent methods creating population inversion by electric discharge or collisions in a buffer gas are not useful. We have focused our attention on the possibility of obtaining inversion of population in a sodium vapor. In literature it has been reported light amplification at the 589-nm line in a dense sodium vapor excited by laser pulses tuned near the $3S \rightarrow 4P$ transition ($\lambda = 330$ nm) [30]. In these circumstances the Na($4P$) atoms are depopulated as a results of cascade-stimulated emission. The same cascades populate the Na($3P$) atoms so efficiently that the inversion of population between the $3P$ and the $3S$ occurs. The duration of the 330-nm light pulse, obtained by frequency-doubling of pulses from a dye laser, was only 7 ns and the population inversion was obtained only for some tens

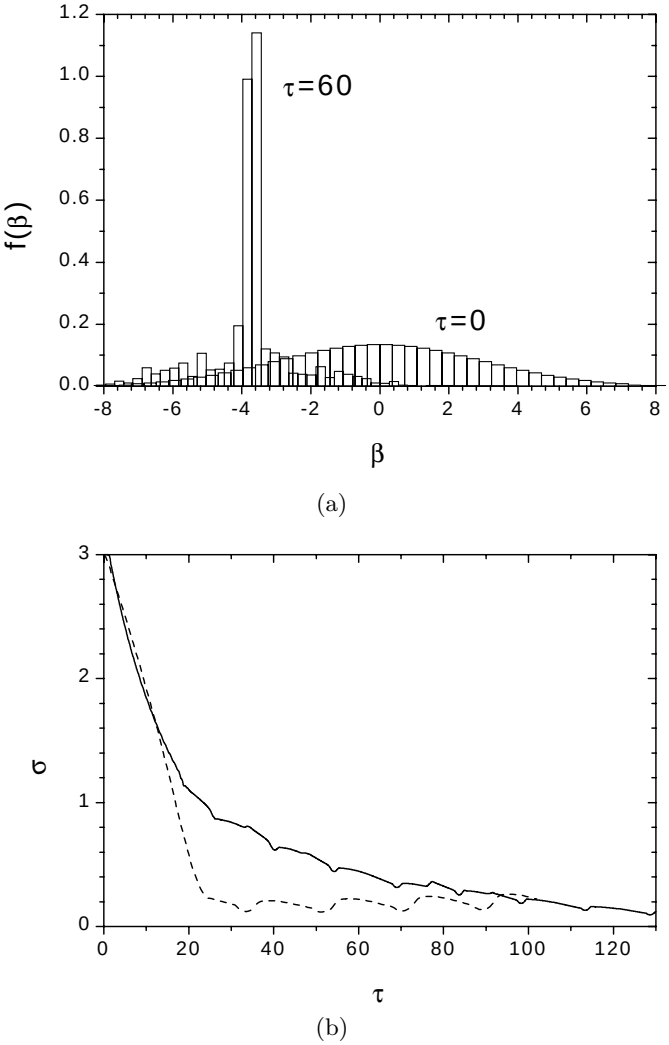

Fig. 17. (a): Histograms of the velocity distribution $f(\beta)$ *vs.* β as obtained from the multi-particle simulation of Figure 15, at $\tau = 60$ and $\tau = 0$. (b): σ *vs.* τ for $\tau_r = 2$ and the other parameters as in Figure 15, as calculated from the exact equations (continuous line) and from the reduced equation (dashed line).

of ns, whereas the typical time required to observe recoil effects is of the order of tens of μs. Nevertheless, we have estimated which should be the typical parameters in an experiment where steady-state population inversion could be created between the $3S$ and $3P$ levels or the $4S$ and $4P$ levels in a sodium vapor.

In the first case, $3S \rightarrow 3P$ ($\lambda = 589$ nm), the recoil frequency is $\omega_r = 6.3 \times 10^5$ s^{-1}, the recoil time is $t_r \approx 3$ μs and $\gamma_\perp = \gamma_\parallel/2 = 3.1 \times 10^7$ s^{-1} We assume an optical cavity with $L_{cav} = 1$ m and $\kappa_c = 0.1\ \gamma_\parallel$, with a quality factor $Q = 5 \times 10^8$. The instability of the unidirectional solution can be observed for $\sigma \leq 2$, which corresponds to a thermal rms velocity σ_v less than 6 m/s and a vapor temperature less than 94 mK. The average velocity threshold is of the order of 3 m/s and the atomic drift along the z-axis is less than 10 μm in one recoil time t_r. Assuming that the length of the vapor cell is $L_s = 1$ cm, a gain-to-loss ratio $g_0 = 100$ can be achieved with a sample density of about 10^9 atoms/cm^3. The vapor can be spontaneously cooled down to the temperature limit of $T_{Dop} = 240$ μK.

We have considered also as a possible example the transition $4S \rightarrow 4P$ ($\lambda = 2210$ nm) for sodium atoms, with recoil frequency $\omega_r = 4.5 \times 10^4$ s^{-1}. Neglecting the relatively very weak spontaneous transition $4P \rightarrow 3D$, the scheme is that of a four-level atom. A calculation similar to that presented in appendix A shows that a pump laser tuned at the $3S \rightarrow 4P$ transition with $I_0 \approx 100$ mW/cm^2 produces population inversion between the $4S$ and $4P$ levels, with $D^{eq} = -0.16$ and $\gamma_\parallel = 2\gamma_\perp = 6.8 \times 10^7$ s^{-1}. In this case, from the condition $\sigma < 2$ it follows that the thermal velocity must be less than 24 m/s, *i.e.* $T < 1.6$ K, whereas the temperature limit is $T_{Dop} = 260$ μK. The average velocity threshold is 12 m/s and the atomic drift along the z-axis about 1 mm in one recoil time t_r. The larger recoil time and velocity threshold require a larger vapor cell. Assuming $L_s = 10$ cm and the same optical cavity as before, a gain-to-loss ratio equal 100 requires a sample density of about 10^7 atoms/cm^3. We note that a stable bidirectional emission can be achieved also with a steady-state flow of cold atoms through the cavity.

In conclusion, we have presented a study of the effect of the atomic motion in a bidirectional ring laser in which the active medium is a cold atomic vapor with Gaussian inhomogeneous broadening. We have studied how the atomic velocity, due either to recoil or thermal motion, influences the stability of the unidirectional and bidirectional emissions. These effects are due to the Doppler shift of the resonance frequency caused by the recoil motion. When the splitting of the two effective resonant frequencies seen by the two counter-propagating fields becomes of the order of the linewidth $\gamma_\perp$, the two modes propagate uncoupled inside the ring cavity. The time scale of the variation of the atomic velocity is of the order of the inverse of the recoil frequency ω_r, whereas the time scale of variation of the mode intensity is of the order of the photon lifetime in the cavity, $(2\kappa_c)^{-1}$. We have found that the unidirectional emission is unstable if either the average velocity and the velocity distribution width are larger than a threshold value. If the mode frequency is resonant with the atoms, the bidirectional emission is stable, whereas if the mode frequency is blue-detuned, unidirectional emission in alternately opposite directions is observed. The results of the stability analysis are in a good agreement with the observed behavior obtained by numerical integration of the dynamical equations. Finally, we have shown that a warm atomic vapor can experience a continuous self-cooling down to the Doppler-cooling limit temperature.

Appendix A: Population inversion

It is well known that population inversion cannot be achieved by resonant absorption of light at the transition frequency of two states. However, a population difference can be achieved for levels a and b (see Fig. 2) by experiments that makes use of three levels. We consider the

$$x_+ = g_0 \int \mathrm{d}\beta f(\beta) \frac{(1+\delta^2+\beta^2)x_+ + 2\delta\beta x_- + \sqrt{x_+^2 - x_-^2}C_+}{1+2(\delta^2+\beta^2)+(\delta^2-\beta^2)^2 + 2g_0[(1+\delta^2+\beta^2)x_+ + 2\delta\beta x_- + \sqrt{x_+^2-x_-^2}C_+]} \tag{79}$$

$$x_- = g_0 \int \mathrm{d}\beta f(\beta) \frac{(1+\delta^2+\beta^2)x_- + 2\delta\beta x_+ + \delta\sqrt{x_+^2 - x_-^2}C_-}{1+2(\delta^2+\beta^2)+(\delta^2-\beta^2)^2 + 2g_0[(1+\delta^2+\beta^2)x_+ + 2\delta\beta x_- + \sqrt{x_+^2-x_-^2}C_+]} \tag{80}$$

$$g_0 \int \mathrm{d}\beta f(\beta) \frac{1+\delta^2+\beta^2+C_+}{1+2(\delta^2+\beta^2)+(\delta^2-\beta^2)^2 + 2g_0 x[1+\delta^2+\beta^2+C_+]} = 1 \tag{81}$$

$$\delta \int \mathrm{d}\beta f(\beta) \frac{2\beta + C_-}{1+2(\delta^2+\beta^2)+(\delta^2-\beta^2)^2 + 2g_0 x[1+\delta^2+\beta^2+C_+]} = 0. \tag{82}$$

states a and b as excited states and the state g as the ground state. A laser beam is used to excite the transition $g \to b$ with a pump rate λ. An atom in level b decays to levels a or g with spontaneous rates γ_{ab} and γ_{bg}, whereas an atom in the level a decays to the level g with spontaneous rate γ_{ag}. We assume $\rho_{gg} + \rho_{aa} + \rho_{bb} = 1$, where ρ_{ii} is the probability of occupation of the ith level. The rate equations for the three levels are:

$$\dot{\rho}_{gg} = -\lambda(\rho_{gg} - \rho_{bb}) + \gamma_{bg}\rho_{bb} + \gamma_{ag}\rho_{aa}, \tag{71}$$

$$\dot{\rho}_{aa} = \gamma_{ab}\rho_{bb} - \gamma_{ag}\rho_{aa}, \tag{72}$$

$$\dot{\rho}_{bb} = \lambda(\rho_{gg} - \rho_{bb}) - (\gamma_{bg} + \gamma_{ab})\rho_{bb}. \tag{73}$$

We introduce $D = \rho_{bb} - \rho_{aa}$ and $D_0 = \rho_{aa} - \rho_{gg}$ as the population differences between the transitions $a \to b$ and $g \to a$. As the transition $g \to a$ is not driven by the radiation in the cavity, we can set the time derivative of D_0 equal to zero in the steady state, and arrive to the following equation for the population difference of the driven transition $a \to b$:

$$\dot{D} = -\gamma_{\parallel}(D - D^{\mathrm{eq}}) \tag{74}$$

where

$$\gamma_{\parallel} = \frac{3\lambda(2\gamma_{ag} + \gamma_{ab}) + 3\gamma_{ag}(\gamma_{ab} + \gamma_{bg})}{3\lambda + 2\gamma_{ag} - \gamma_{ab} + \gamma_{bg}} \tag{75}$$

$$D^{\mathrm{eq}} = \frac{\lambda(\gamma_{ag} - \gamma_{ab})}{\lambda(2\gamma_{ag} + \gamma_{ab}) + \gamma_{ag}(\gamma_{ab} + \gamma_{bg})}. \tag{76}$$

It is evident from equation (76) that in order for D^{eq} to be positive, *i.e.* ρ_{bb} larger than ρ_{aa}, the condition $\gamma_{ab} < \gamma_{ag}$ must be satisfied. In words, the atoms excited into state b must decay relatively slowly into state a, from where they drop rapidly back into the ground state g. For strong pumping ($\lambda \gg \gamma_{ab} + \gamma_{bg}$),

$$\gamma_{\parallel} \approx 2\gamma_{ag} + \gamma_{ab} \tag{77}$$

$$D^{\mathrm{eq}} \approx \frac{\gamma_{ag} - \gamma_{ab}}{2\gamma_{ag} + \gamma_{ab}}. \tag{78}$$

We note that the maximum possible value for D is $1/2$, when the transition between the states g and b approaches saturation and when $\gamma_{ab} \ll \gamma_{ag}$.

Appendix B: Bidirectional stationary solutions

We discuss in detail the general form of the stationary bidirectional solutions. Introducing $x_\pm = (x_1 \pm x_2)/2$ and setting the time derivative equal to zero, equation (36) may be written as:

see equations (79, 80) above,

where $C_+ = (1+\delta^2+\beta^2)\mathrm{Re}z_0 + \beta(1-\delta^2+\beta^2)\mathrm{Im}z_0$ and $C_- = 2\beta\mathrm{Re}z_0 - (1+\delta^2-\beta^2)\mathrm{Im}z_0$. From equations (79) and (80), the symmetric bidirectional solution, with $x_- = 0$ (*i.e.* $x_1 = x_2$) and $x_+ = x$, must satisfy the following two equations:

see equations (81, 82) above.

Equation (82) is always satisfied when $\delta = 0$, so the symmetric bidirectional solution may exist in the resonant regime. In the detuned regime, with $\delta \neq 0$, equation (82) can never be true for Doppler broadening, whereas it may be satisfied for homogeneous broadening and $\beta_0 = 0$, *i.e.* for $f(\beta) = \delta(\beta)$. In fact, $\beta = 0$ implies that $\mathcal{L}_{n,m} = 1$, $\alpha_n = 1 + 2g_1 x$ and $\beta_n = g_1 x$, where $g_1 = g_0/(1+\delta^2)$. From equation (31) it follows that z_0 is real, so that $C_- = 0$ and equation (82) is satisfied. Furthermore, equation (31) becomes independent on n and can be solved explicitly, giving $z_0 = (\sqrt{1 + 4g_1 x + 8g_1^2 x^2} - 1 - 2g_1 x)/2g_1 x$. From equation (81) it is straightforward to demonstrate that the bidirectional solution is

$$x = \frac{1}{2}\left[1 - \frac{1}{4g_1}\left(1 + \sqrt{1+8g_1}\right)\right]. \tag{83}$$

From equation (33), it follows also that $d_0 = D^{\rm eq}/\sqrt{1+4g_1x}$ and, as $d_n = z_0^n d_0$,

$$D(\theta) = d_0\left[1+\sum_{n=1}^{\infty} z_0^n {\rm e}^{{\rm i}n\theta} + {\rm c.c.}\right] = \frac{D^{\rm eq}}{1+4g_1x\cos^2(\theta/2)}.$$

A stability analysis shows that the bidirectional solution (83) is unstable. In fact, linearizing the motion equations for x_+ and x_- around (83), assuming $x_+ = x+\epsilon_+$ and $x_- = \epsilon_-$ with $\epsilon_\pm \propto \exp(\lambda_\pm \tau)$, it is easy to show that $\lambda_+ = \lambda_- = (\sqrt{1+8g_1}-3)/4$, which is positive for $g_1 > 1$.

We now discuss the general stationary solutions in the resonant regime. When $\delta = 0$, equations (79) and (80) simplifies into:

$$x_+ = g_0\int {\rm d}\beta f(\beta)\frac{x_+ + \sqrt{x_+^2-x_-^2}\,Z}{1+\beta^2+2g_0[x_+ + \sqrt{x_+^2-x_-^2}\,Z]} \quad (84)$$

$$x_- = g_0 x_- \int {\rm d}\beta \frac{f(\beta)}{1+\beta^2+2g_0[x_+ + \sqrt{x_+^2-x_-^2}\,Z]}, \quad (85)$$

where $Z = {\rm Re}z_0 + \beta{\rm Im}z_0$. Equation (85) is satified either for $x_- = 0$ and $x_+ = x$ (which is a particular case of the symmetric bidirectional solution discussed before), where x is the solution of the implicit equation

$$g_0\int {\rm d}\beta f(\beta)\frac{1+Z}{1+\beta^2+2g_0x[1+Z]} = 1, \quad (86)$$

or for $x_- \neq 0$ and

$$g_0\int {\rm d}\beta \frac{f(\beta)}{1+\beta^2+2g_0[x_+ + \sqrt{x_+^2-x_-^2}\,Z]} = 1,$$

which, once substituted into equation (84), implies

$$\sqrt{x_+^2-x_-^2}\int {\rm d}\beta \frac{f(\beta)Z}{1+\beta^2+2g_0[x_+ + \sqrt{x_+^2-x_-^2}\,Z]} = 0.$$

This last equation is satisfied when $x_+ = \pm x_-$, *i.e.* when either $x_2 = 0$ or $x_1 = 0$ (unidirectional solution), or for $x_+^2 \neq x_-^2$, when the following two equations are satisfied:

$$\int {\rm d}\beta \frac{f(\beta)Z}{1+\beta^2+2g_0[x_+ + \sqrt{x_+^2-x_-^2}\,Z]} = 0 \quad (87)$$

$$g_0\int {\rm d}\beta \frac{f(\beta)}{1+\beta^2+2g_0[x_+ + \sqrt{x_+^2-x_-^2}\,Z]} = 1. \quad (88)$$

This last case corresponds to the asymmetric bidirectional solution, with $x_1 \neq x_2$ and both x_1 and x_2 different from zero, and it exists only for inhomogeneous broadening.

In conclusion, the symmetric bidirectional solution may exist either in the resonant regime or, in the case of homogeneous broadening, when $\delta \neq 0$ and $\beta_0 = 0$ (but in this last case is unstable). The asymmetric bidirectional solution may exist in the following three cases: (a) detuned regime with inhomogeneous broadending; (b) detuned regime with homogeneous broadening and $\beta_0 \neq 0$; (c) resonant regime with inhomogeneous broadening, if equations (87) and (88) are simultaneously satisfied.

Appendix C: Evaluation of C_0 in equation (56)

Assuming resonance, $\delta = 0$, and using (29), equations (25) and (26) become

$$\alpha_n = 1 + 2{\rm i}n\gamma\beta + g_0[\xi_n + \xi_{n+1}]x_+$$
$$\beta_n = g_0\xi_n\sqrt{x_+^2-x_-^2}$$

where $\xi_n = (1+{\rm i}(2n-1)\beta)^{-1}$. Assuming $x_+ = x_0+\epsilon_+$ and $x_- = \epsilon_-$, we expand z_n in equation (31) up to the first order of ϵ_+ and ϵ_-, obtaining $z_n \sim z_n^{(0)} + c_n\epsilon_+$, where $z_n^{(0)}$ is the zero-order term and

$$c_{n-1} = A_n c_n + B_{n-1}, \quad (89)$$

where $A_n = [z_{n-1}^{(0)}]^2(\xi_{n+1}/\xi_n)$ and $B_n = -\{[1+2{\rm i}(n+1)\gamma\beta]/g_0x_0^2\}[z_n^{(0)}]^2/\xi_{n+1}$. Equation (89) can be solved numerically by iteration to give $c_0 = B_0 + A_1B_1 + A_1A_2B_2...$ Finally, $Z = {\rm Re}z_0 + \beta{\rm Im}z_0 = Z_0 + C_0\epsilon_+$, where $Z_0 = {\rm Re}z_0^{(0)} + \beta{\rm Im}z_0^{(0)}$ and $C_0 = {\rm Re}c_0 + \beta{\rm Im}c_0$.

References

1. R. Bonifacio, L. De Salvo, Nucl. Instrum. Meth. Phys. Rev. A **341**, 360, (1994); R. Bonifacio, L. De Salvo, L.M. Narducci, E.J. D'Angelo, Phys. Rev. A **50**, 1716 (1994).
2. R. Bonifacio, G.R.M. Robb, B.W.J. McNeil, Phys. Rev. A **56**, 912 (1997) and references therein.
3. J. Guo, P.R. Berman, B. Dubetsky, P.R. Berman, Phys. Rev. A **46**, 1426 (1992); J.Y. Courtois, G. Grynberg, B. Louinis, P. Verkerk, Phys. Rev. Lett. **72**, 3017 (1994).
4. P.R. Berman, Phys. Rev. A **59**, 585 (1999).
5. R. Bonifacio, B.W.J. McNeil, N. Piovella, G.R.M. Robb, Phys. Rev. A **61**, 023807 (2000).
6. R. Bonifacio, B.W.J. McNeil, N. Piovella, G.R.M. Robb, Opt. Commun. **194**, 151 (2001).
7. R. Bonifacio, B.W.J. McNeil, G.R.M. Robb, Phys. Rev. A **61**, 031801(R) (2000).
8. R. Bonifacio, B.W.J. McNeil, N. Piovella, G.R.M. Robb, Opt. Commun. **179**, 559 (2000).
9. B.W.J. McNeil, G.R.M. Robb, R. Bonifacio, N. Piovella, Europhys. Lett. **49**, 316 (2000).
10. R. Bonifacio, B.W.J. McNeil, G.R.M. Robb, Opt. Commun. **161**, 1 (1999).
11. L.N. Menegozzi, W.E. Lamb Jr, Phys. Rev. A **8**, 2103 (1973).
12. P. Mandel, G.P. Agrawal, Opt. Commun. **42**, 269 (1982).
13. H. Zeghalche, P. Mandel, N.B. Abraham, L.M. Hoffer, G.L. Lippi, T. Mello, Phys. Rev. A **37**, 470 (1988) and references therein.

14. See *e.g.* P. Mandel, *Theoretical problems in cavity nonlinear optics*, in *Cambridge Studies in Modern Optics* (Cambridge University Press, Cambridge, 1997).
15. W.W. Chow, J. Gea-Banacloche, L.M. Pedrotti, V.E. Sanders, M.O. Scully, Rev. Mod. Phys. **57**, 61 (1985).
16. See *e.g.* R.W. Boyd, M.G. Rayner, L.M. Narducci, *Optical instability. Proceeding Rochester 1985*, in *Cambridge Studies in Modern Optics* (Cambridge University Press, Cambridge, 1986).
17. P. Mandel, H. Zeghlache, Opt. Commun. **47**, 146 (1983).
18. W. Ketterle, Physics Today, December, 30 (1999).
19. M.G. Moore, P. Meystre, Phys. Rev. A **58**, 3248 (1998).
20. N. Piovella, M. Gatelli, R. Bonifacio, Opt. Commun. **194**, 167 (2001).
21. S. Inouye, A.P. Chikkatur, D.M. Stamper-Kurn, J. Stenger, D.E. Pritchard, W. Ketterle, Science **285**, 571 (1999).
22. F.T. Arecchi, R. Bonifacio, IEEE J. Quant. Electron. **1**, 169 (1965).
23. P.R. Hemmer, N.P. Bigelow, D.P. Katz, M.S. Shahriar, L. De Salvo, R. Bonifacio, Phys. Rev. Lett. **77**, 1468 (1996).
24. S. Stenholm, W.E. Lamb Jr, Phys. Rev. **181**, 618 (1969).
25. N.B. Abraham, L.A. Lugiato, P. Mandel, J. Opt. Soc. Am. B **2**, 35 (1985).
26. Z. Ye, L.M. Narducci, Phys. Rev. **63**, 043815-1 (2001).
27. S. Chu, L. Hollberg, J. Bjorkholm, A. Cable, A. Ashkin, Phys. Rev. Lett. **55**, 48 (1985).
28. See W.D. Phillips, in *Laser Manipulation of Atoms and Ions*, *Proc. S.I.F., Course CXVIII*, edited by E. Arimondo, W.D. Phillips, F. Strumia (North Holland, Amsterdam, 1992), p. 289, and references therein.
29. S. Stenholm, Rev. Mod. Phys. **58**, 699 (1986).
30. T. Stacewicz, N.A. Gorbunov, P. Kozlowski, Appl. Phys. B **66**, 461 (1998).